FULL PAPERS

Gets into your head: By using a structure-guided drug discovery approach, highly selective brain-penetrant Plk-2 inhibitors were designed with the use of an interesting aromatic edge–face interaction as a potency–selectivity determinant. An analogue from this work lowered phosphorylated α-synuclein levels in vivo on oral dosing, demonstrating successful target engagement in the rat brain and paving the way for proof-of-concept studies in rodent models of Parkinson's disease.

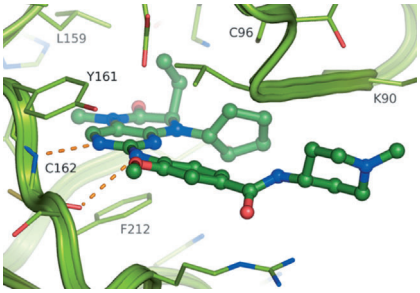

*D. L. Aubele, R. K. Hom, M. Adler, R. A. Galemmo, Jr., S. Bowers, A. P. Truong, H. Pan, P. Beroza, R. J. Neitz, N. Yao, M. Lin, G. Tonn, H. Zhang, M. P. Bova, Z. Ren, D. Tam, L. Ruslim, J. Baker, L. Diep, K. Fitzgerald, J. Hoffman, R. Motter, D. Fauss, P. Tanaka, M. Dappen, J. Jagodzinski, W. Chan, A. W. Konradi, L. Latimer, Y. L. Zhu, H. L. Sham, J. P. Anderson, M. Bergeron, D. R. Artis**

■■ – ■■

Selective and Brain-Permeable Polo-like Kinase-2 (Plk-2) Inhibitors That Reduce α-Synuclein Phosphorylation in Rat Brain

DOI: 10.1002/cmdc.201300166

Selective and Brain-Permeable Polo-like Kinase-2 (Plk-2) Inhibitors That Reduce α-Synuclein Phosphorylation in Rat Brain

Danielle L. Aubele,[a] Roy K. Hom,[a] Marc Adler,[a] Robert A. Galemmo, Jr.,[a, d] Simeon Bowers,[a] Anh P. Truong,[a] Hu Pan,[a] Paul Beroza,[a] R. Jeffrey Neitz,[a, e] Nanhua Yao,[a] May Lin,[a] George Tonn,[b] Heather Zhang,[b] Michael P. Bova,[a] Zhao Ren,[a] Danny Tam,[a] Lany Ruslim,[a] Jeanne Baker,[a] Linnea Diep,[a] Kent Fitzgerald,[b] Jennifer Hoffman,[b] Ruth Motter,[b] Donald Fauss,[a] Pearl Tanaka,[b] Michael Dappen,[a] Jacek Jagodzinski,[a] Wayman Chan,[a] Andrei W. Konradi,[a] Lee Latimer,[a] Yong L. Zhu,[a] Hing L. Sham,[a] John P. Anderson,[c] Marcelle Bergeron,[b] and Dean R. Artis*[a]

Polo-like kinase-2 (Plk-2) has been implicated as the dominant kinase involved in the phosphorylation of α-synuclein in Lewy bodies, which are one of the hallmarks of Parkinson's disease neuropathology. Potent, selective, brain-penetrant inhibitors of Plk-2 were obtained from a structure-guided drug discovery approach driven by the first reported Plk-2–inhibitor complexes. The best of these compounds showed excellent isoform and kinome-wide selectivity, with physicochemical properties sufficient to interrogate the role of Plk-2 inhibition in vivo. One such compound significantly decreased phosphorylation of α-synuclein in rat brain upon oral administration and represents a useful probe for future studies of this therapeutic avenue toward the potential treatment of Parkinson's disease.

Introduction

Lewy Bodies are intracytoplasmic inclusions found in dopaminergic neurons and are recognized as the prime histological marker of Parkinson's disease. They are prognostic of Parkinson's disease dementia, dementia with Lewy bodies, multiple system atrophy, and Lewy body dysphagia.[1] α-Synuclein is the major component of Lewy bodies,[1] where it is found to be highly phosphorylated at serine 129.[2] Our research group has demonstrated,[3] and others have confirmed,[4] that polo-like kinase-2 (Plk-2) is the major enzyme responsible for phosphorylation of α-synuclein at serine 129, thereby suggesting that Plk-2 may play a key role in the progression of Parkinson's-like pathologies. To examine this hypothesis, we aimed at creating highly selective inhibitors of Plk-2 for use as chemical probes in various cellular and in vivo models of α-synucleinopathy.[5] A robust co-crystallization system was obtained, leading to the first reported small-molecule complexes with the Plk-2 kinase domain. This enabled a computationally assisted, structure-guided approach that yielded a series of compounds with excellent kinome selectivity, including selectivity for Plk-2 over Plk-1 and Plk-3. Many of these compounds displayed reasonable cellular potency, and optimization yielded **21**, which had suitable physicochemical and pharmacokinetic properties to demonstrate in vivo decreases in phospho-S129 α-synuclein levels in rat brain upon oral dosing.

The polo-like kinase family is characterized by the presence of the polo-box domain, a conserved motif with roles in protein–protein binding and modulation of the kinase domain activity.[6] This family has drawn a great deal of interest for its varied and critical roles in control of the cell cycle.[6,7] Plk-1 is the most studied as a potential target for cancer therapeutics,[8] and X-ray crystal structures have been published for the Plk-1 kinase domain.[9] The functions remain less clear for the other members of the family: Plk-2 (or serum-inducible kinase, Snk), Plk-3, Plk-4, and particularly the recently identified Plk-5, which lacks a functional kinase domain.[10]

[a] Dr. D. L. Aubele, Dr. R. K. Hom, Dr. M. Adler, Dr. R. A. Galemmo, Jr., Dr. S. Bowers, Dr. A. P. Truong, Dr. H. Pan, Dr. P. Beroza, Dr. R. J. Neitz, Dr. N. Yao, M. Lin, Dr. M. P. Bova, Dr. Z. Ren, D. Tam, L. Ruslim, Dr. J. Baker, L. Diep, D. Fauss, Dr. M. Dappen, Dr. J. Jagodzinski, W. Chan, Dr. A. W. Konradi, Dr. L. Latimer, Dr. Y. L. Zhu, Dr. H. L. Sham, Dr. D. R. Artis
Molecular Discovery, Elan Pharmaceuticals
180 Oyster Point Boulevard, South San Francisco, CA 94080 (USA)
E-mail: drartis@comcast.net

[b] Dr. G. Tonn, H. Zhang, Dr. K. Fitzgerald, J. Hoffman, R. Motter, P. Tanaka, Dr. M. Bergeron
Pharmacological Sciences, Elan Pharmaceuticals
180 Oyster Point Boulevard, South San Francisco, CA 94080 (USA)

[c] Dr. J. P. Anderson
Department of Biology, Elan Pharmaceuticals
180 Oyster Point Boulevard, South San Francisco, CA 94080 (USA)

[d] Dr. R. A. Galemmo, Jr.
Current address: Southern Research Institute
2000 Ninth Avenue South, Birmingham, AL 35205 (USA)

[e] Dr. R. J. Neitz
Current address: Small-Molecule Discovery Center
University of California San Francisco, San Francisco, CA 94158 (USA)

Supporting information for this article is available on the WWW under http://dx.doi.org/10.1002/cmdc.201300166.

Neither Plk-3 nor Plk-2 function is essential, as knockout mice are viable.[11] In addition to α-synuclein phosphorylation and a putative role in neurodegenerative pathology, Plk-2 is involved in modulation of cell division in the presence of microtubule disruption[12] or mitochondrial impairment.[13] In conjunction with Cdk-5, Plk-2 plays a critical role in neuronal homeostatic plasticity.[14] It is involved in control of excitation-dependent synaptic plasticity resulting in destabilization of postsynaptic structures. This follows the binding or phosphorylation of targets including the spine-associated rap (SPAR) guanosine triphosphatase activating protein[15] and *N*-ethylmaleimide-sensitive fusion protein (NSF).[16] The roles of Plk-3 include regulation of cell-cycle checkpoints,[17] modulation of the response to hypoxia,[11b] and synaptic destabilization.[18] The contribution of Plk-3 to α-synuclein phosphorylation is less clear than for Plk-2; although the in vitro activity of isolated Plk-3 is similar to that of Plk-2, it has not been as extensively validated in vivo.[3,4]

The availability of selective, high-affinity chemical probes for the Plks would be of obvious utility to elucidate their role in cellular functions. For our intended target validation studies, a chemical probe inhibitor with high kinome-wide specificity and isoform selectivity for Plk-2 over the other Plks would be required. To be a useful tool for evaluating the role of Plk-2 in cultured cells and in vivo, it would also be necessary to avoid potentially toxic effects of Plk-1 inhibition in dividing cells, and selectivity for Plk-2 over Plk-3 would eliminate the latter as a potentially confounding mechanistic element. For the evaluation of in vivo activity, a metabolically stable compound that can achieve good CNS exposures in rodents would be required. Our efforts resulted in two closely related series of compounds that have enabled in vivo studies yielding encouraging data, and a portion of the compounds derived from this work, resulting from a focused sub-series SAR expansion, have been described separately.[19]

Results and Discussion

The known Plk inhibitor BI 2536 (**1**),[8,20] a clinical oncology pteridinone with a moderate level of selectivity over other kinase families and IC_{50} values in the low nanomolar range for Plk-1–3 (Figure 1 a), provided an excellent starting point for the development of Plk-2-specific inhibitors.[21] The co-crystal structure of Plk-1 with **1** in the ATP binding site has been reported, along with analysis of the important binding contacts and a hypothesis for the observed kinase selectivity and potency. The location of the *ortho*-methoxy substituent of the aniline side chain of **1** in a pocket created by the gatekeeper+2 residue Leu132 served as a steric constraint that attenuated activity for kinases with a larger Phe or Tyr at this position. The reported selectivity data at 1 mM concentration of **1** against a panel of 21 kinases supported this model. The only exception was Plk-2, a Plk isoform with Tyr at the gatekeeper+2 position. The authors argued that **1** was active against Plk-1–3 because the related active sites provided many similar productive interactions with **1** across all three isoforms.[21]

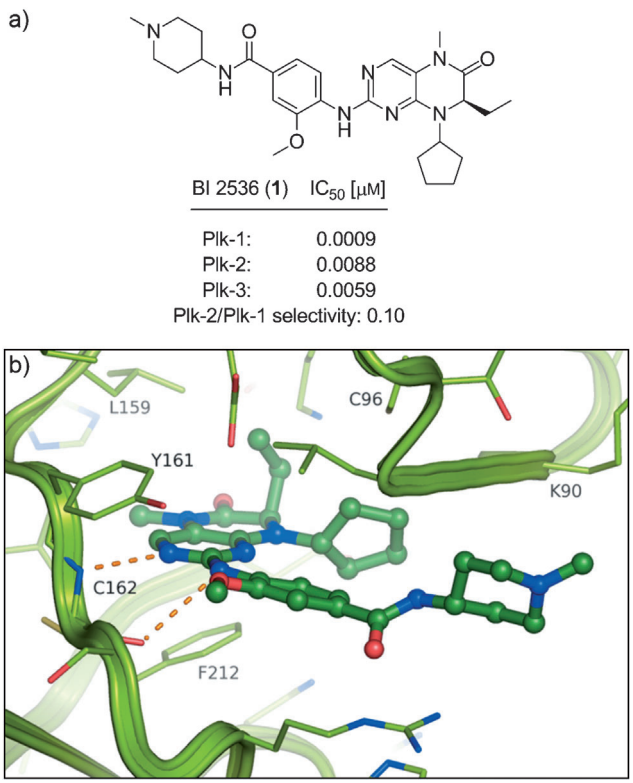

Figure 1. a) Biochemical potency of **1** against Plk-1–3. b) Crystal structure of **1** bound to Plk-2 (PDB code 4I5M, 1.8 Å resolution).

Based on this information, it appeared likely that with sufficient structural information, selective, high-affinity analogues targeting Plk-2 could be obtained from the pteridinone scaffold. We were particularly interested in exploiting the Leu-to-Tyr difference at position 161 that differentiates Plk-2 from Plk-1 and -3, and reasoned that exploiting this change could provide the means to obtain isoform-selective analogues. To this end, a crystal structure of **1** with the kinase domain of Plk-2 was obtained (Figure 1 b). This crystal structure represented the first published structure for Plk-2 (PDB code 4I5M). Many of the binding interactions corresponded to contacts reported previously[21] for **1** with Plk-1 (PDB code 2RKU). Critically, the central amide in the hinge, Cys162, donates a hydrogen bond to the pteridinone N1 atom (2.9 Å). This mimics the interaction of the N1 purine of adenosine with Plk-1 (PDB code 2OU7). There were several other interactions that mimic the binding of **1** to Plk-1 and likely contribute to the observed selectivity against a broad range of kinases: 1) the 5-methyl group is packed against the gatekeeper Leu159, 3.9 Å away; 2) the 6-carbonyl tied into the water network in the specificity pocket; 3) the 7-ethyl substituent is in close contact with Cys96 (Sγ, 3.9 Å) in the P-loop; 4) the 8-cyclopentane ring induces a conformational change in the P-loop that results in a close contact with the backbone of Lys90 (4.2 Å); and 5) the pteridinone ring is packed against the side chain of Phe212 (3.5 Å).

The most notable difference between Plk-1 and Plk-2 around the compound involves the aforementioned Leu–Tyr substitution in the middle of the hinge (residues Leu132 and

Tyr161, respectively). Due to a slight shift in the orientation of residues adjacent to Tyr161, the hinge backbone is further from the inhibitor than in Plk-1, with a maximum displacement of 0.7 Å at the Tyr161 Cα carbon position. This results in small adjustments of the two hydrogen bonds to the hinge at Cys162. In addition, while the *ortho*-methoxy group in **1** is fairly well packed against Leu132 in Plk-1, it exhibits a steric clash with the side chain of Tyr161 in Plk-2 (3.3 Å). This likely contributes to the ~10-fold loss in potency against Plk-2 relative to that observed against Plk-1.

We reasoned that the portion of the inhibitor near Tyr161 is likely not optimally engineered for Plk-2 potency. To examine this further, we used compound **1a**, a fragment of **1** consisting of the pteridinone core without the aniline side chain. Although this results in a loss of more than half the atoms in the inhibitor, the potency of this compound is decreased by only 130-fold. In addition, compound **1a** shows equipotent activity against both Plk-2 and Plk-1, representing a 10-fold improvement in relative selectivity and supporting the idea that the *ortho*-methoxy substituent represents a negative binding determinant for Plk-2. The crystal structure of Plk-2 with compound **1a** revealed that the pteridinone core maintains almost all of the binding interactions of the larger compound (Figure 2a, PDB code 4I6B).

Based on this analysis, we formed the hypothesis that the interaction of the pteridinone **1a** with Plk-2 would be improved by forming an edge-to-face interaction with the aryl side chain of Tyr161. Modeling studies (see below) suggested that either a five- or six-membered ring attached to the 2-position through a biaryl linkage could be accommodated. To test this hypothesis we synthesized the series of heterocyclic analogues listed in Table 1. The 2-pyrrole ring analogue **4** has improved potency and selectivity relative to **1a**, and was the first to be examined structurally. A crystal structure of **4** in Plk-2 (PDB code 4I5P) revealed a clear edge-to-face[22] interaction between the 2-pyrrole group and Tyr161, indicated by: 1) close contact (3.5 Å) between the C3/C4 edge of the pyrrole moiety and the 4-hydroxyphenyl side chain of Tyr161; 2) the fact that the alignment of the edge of the pyrrole ring with the center of the hydroxyphenyl group of Tyr161 resides in an "offset T" relationship, consistent with the energy minima for an edge-to-face interaction predicted by benzene dimer model calculations.[23] However, the shallow approach angle (58°) of the pyrrole ring in **4** to the Tyr161 hydroxyphenyl group was a substantial deviation from the optimal 90° angle predicted by this model. The five-membered pyrrole ring of **4** was nearly coplanar with the pteridinone, perhaps due to the intramolecular hydrogen bond between the pyrrole NH and N1 of the pteridi-

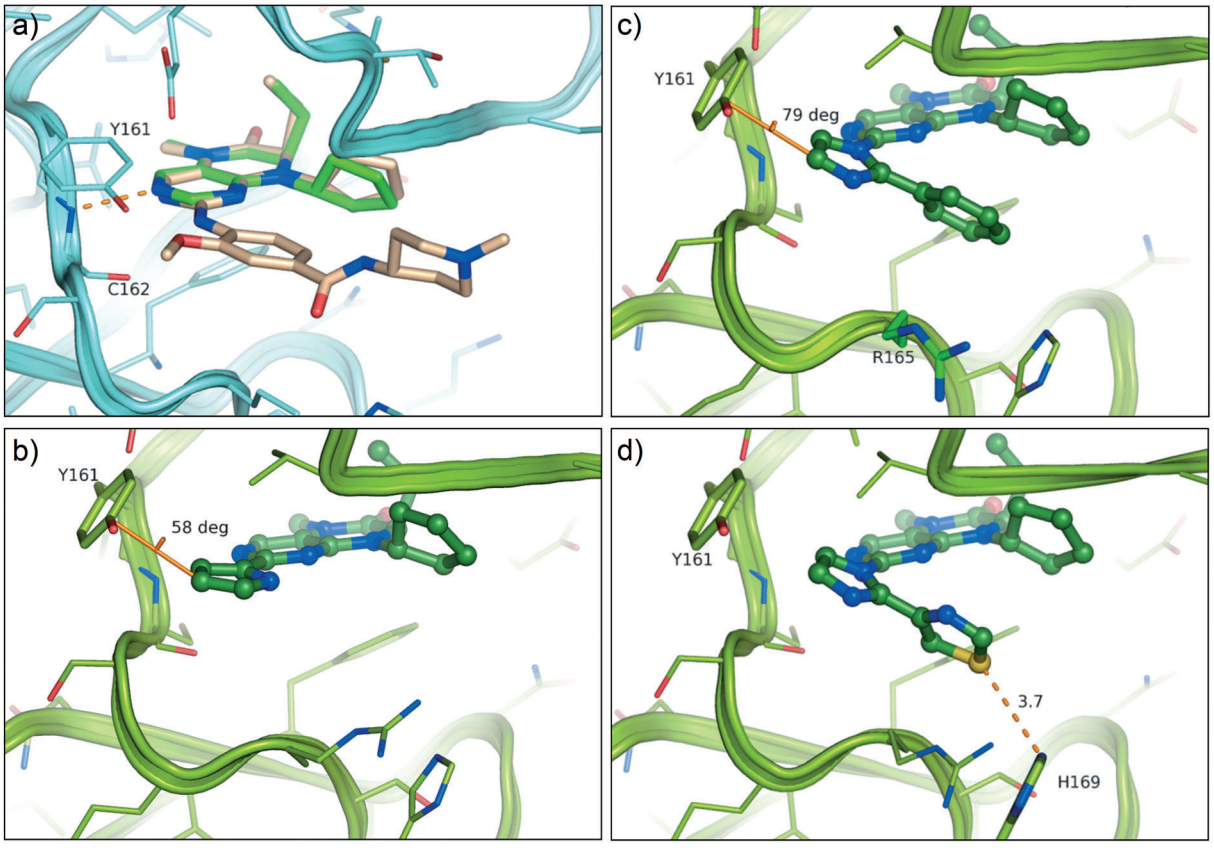

Figure 2. Crystal structures of four inhibitors bound to Plk-2. a) Compound **1a**: PDB code 4I6B, 1.8 Å resolution; the protein is shown with cyan carbon atoms, compound **1a** in green, and the superimposed structure of **1** in pink. b) Compound **4**: PDB code 4I5P, 1.7 Å resolution; the edge-to-face angle for the Tyr161/pyrrole interaction is highlighted with an orange line. c) Compound **9**: PDB code 4I6F, 2.9 Å resolution, showing the corresponding edge-to-face angle. d) Compound **11**: PDB code 4I6H, 1.9 Å resolution.

Table 1. Enzyme inhibition data and Plk isoform selectivity ratios for compounds **1a**–**7**.

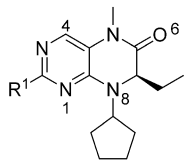

Compd	R^1	IC_{50} [μM][a] Plk-2	Plk-1	Plk-3	Selectivity Plk-2/Plk-1	MetStab (m,r,h)[b]	clog P[c]
1a	H–	1.17	1.45	–	1.1	0, 1, 19	1.9
2		1.24	13.2	–	10.6	0, 0, 0	2.6
3		0.061	0.306	18.618	5.1	66, 5, 85	2.5
4		0.377	1.21	–	3.2	0, 0, 12	2.8
5	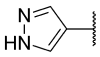	0.10	0.253	–	2.53	12, 11, 52	2.3
6		0.031	0.167	1.464	5.4	0, 0, 22	2.2
7		0.071	0.551	10.772	7.7	4, 5, 20	2.8

[a] Values are means of at least two experiments at 100 mM ATP concentration; details can be found in the Supporting Information. [b] See ref. [23]. [c] Details regarding the method of calculation can be found in the Supporting Information.

none. The rigidity of the two aromatic ring systems affect both the selectivity and potency of **4**. Consequently, our focus was placed on identifying a replacement group that could exhibit more optimal interactions with Tyr161.

The biochemical data for the initial series of seven heterocyclic analogues are listed in Table 1. Considering that **1a** showed Plk-2 $IC_{50} = 1.17$ μM, any derivative in this set with a substantial improvement in Plk-2 inhibition relative to **1a** was likely due to the interaction added by the appended ring. The 5-membered alkyl *N*-pyrrolidine ring analogue **2** represented a variation that approached the activity of **1a**, but did not contribute any favorable binding energy. A series of 5-membered aryl heterocyclic analogues **3**–**7** proved to be potent modifications, with Plk-2 IC_{50} values of 0.377 μM or better. The most potent of these was the 2-(thiazo-5-yl) analogue **6**, with an eightfold increase in potency relative to **1a**.

The selectivity ratios for Plk-2 versus Plk-1 varied from 3- to 11-fold amongst the inhibitors shown in Table 1, the best representing a 100-fold swing in relative potency between Plk-2 and Plk-1 from the starting compound. Plk-3 activity was almost always significantly worse than that for Plk-1, and thus eliminated the issue of potentially confounding biological activity from the landscape of likely optimization issues. Measurements were performed at a single concentration (10 μM) using a panel of 35 kinases chosen to represent a broad sampling of the kinome (Supporting Information table 1). The initial lead, **1**, was included for comparison. Both **1** and **5** demonstrated poor selectivity by inhibiting at least 10 kinases in the panel by 40–100%. The rates of inhibition exceeded 80% for at least three kinases. Kinome selectivity was significantly improved by replacing the 4-pyrazole in **5** with a 4-pyridine in **7**. Compound **7** inhibited only three kinases by >40%, and no kinase showed >50% inhibition, suggesting that this design approach was not inherently likely to result in a dramatic loss of overall kinome selectivity.

The microsomal stability was measured for all of these inhibitors, which generally exhibited poor to moderate oxidative stability across species (mouse, rat, and human).[24] Because the inhibitors **1a**–**7** all showed low lipophilicity (clog $P < 3$), it was surmised that this liability might be due to site-specific oxidation. In the case of the heteroaryl-substituted analogues, this likely meant oxidation at the carbon atom adjacent to a heteroatom within the pendant aromatic ring.

However, among these compounds, imidazole **3** demonstrated a reasonable selectivity profile, with no inhibition greater than 30% for any kinase outside the Plk family, good stability in mouse and human microsomes (but not in rat microsomes), and moderate activity in the Plk-2 cell assay ($IC_{50} = 4.5$ μM). Based on these results, as well as its good solubility and permeability, compound **3** was selected for further analogue-generating efforts.

Throughout this process of design, synthesis, and biochemical and structural characterization, molecular dynamics (MD) simulations were performed to provide a computational prediction of inhibitor binding and complex structure. Once stable simulation systems had been obtained, molecular mechanics Poisson–Boltzmann surface area (MM-PBSA) methods[25] were used to estimate binding energies for new analogues. Generally, reasonable agreement was obtained between computed and experimental structures (Figure 3) and binding affinities (the latter will be the subject of a more detailed report). Compound designs with the most favorable binding energies were

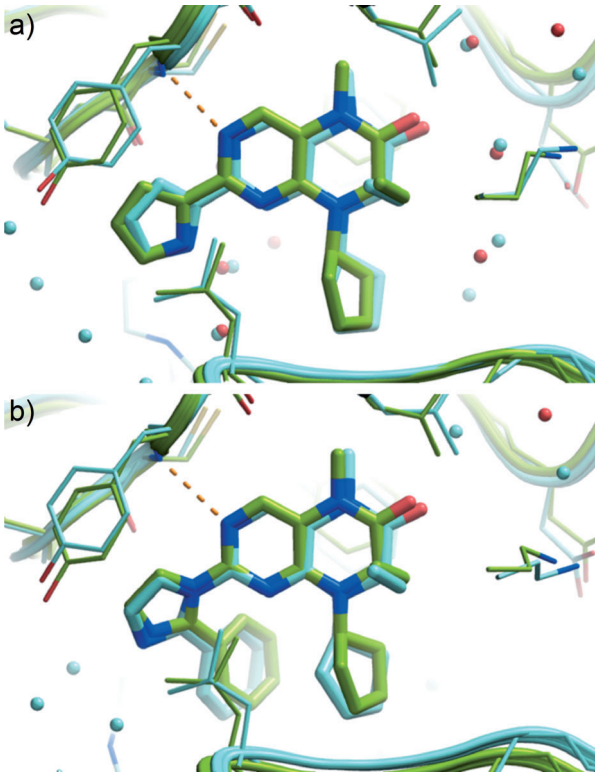

Figure 3. Comparisons of X-ray structures and computational models. X-ray structures are shown with green carbon atoms, and models are colored in cyan (including solvent atoms). The coordinates for the model structure were obtained by hierarchical clustering of the MD frames using the ligand heavy atom coordinates. The MD frame shown is the best representative (i.e., cluster medoid) of the largest cluster: a) compound **4**; b) compound **9**.

prioritized for synthesis, unless otherwise driven by a critical hypothesis or rationale.

Analysis of the structure and subsequent modeling studies highlighted the presence and potential utility of a small cleft below the imidazole 2-position of compound **3**, tucked inside the Cα–Cβ of Arg165 (Figure 2), sufficient to accommodate a five- or six-membered ring. Appropriate substitution at the 2-position of the imidazole enhanced the activity in this series (Table 2). MM-PBSA calculations suggested that appropriate substitution at this site would enhance Plk-2 potency. With a simple methyl substitution in **8**, there was a loss in potency with respect to **3**, but increased selectivity and microsomal stability. However, the addition of a 2′-phenyl ring in **9** provided a 12-fold boost in potency relative to **3**. Examination of **9** in the kinase panel suggested broad kinome selectivity: with the exception of the Plks, **9** did not display any significant kinase inhibition $>40\%$ at a concentration of 10 μM (Supporting Information table 1), suggesting a selectivity window of roughly 1000-fold or more. The crystal structure (Figure 2c, PDB code 4I6F) revealed that compound **9** had a more optimal edge-to-face interaction with Tyr161 (3.5 Å, ∡ 79°). The change in angle reflected the internal stacking of the additional 2′-phenyl substituent against the 8-cyclopentane group. This stacking increased the dihedral angle between the pteridinone and the directly connected imidazole ring (31° in **9** versus 12° for **4**). The 2′-phenyl substituent ring also exhibited a hydrophobic interaction with the side chain of Arg165 (Cγ, 4.0 Å). Surprisingly, and somewhat uniquely in the series, **9** did not demonstrate any selectivity between Plk-1 and Plk-2. Plk-3 activity was still more than 10-fold worse than that for Plk-1. Although it is possible this is partly due to bottom-end compression of the assay due to the Plk-2 concentration used (the final protein concentration is 3 nM, Supporting Information), we did not have the means to pursue this hypothesis further. Because small changes to the molecule resulted in compounds with significant isoform selectivity, our analysis suggested that a practical approach involving fine tuning of the cooperative interaction between the Tyr161/2′-(phenyl)imidazole and Arg165/2′-(phenyl)imidazole/8-cyclopentane ensemble could hold the key to improving selectivity among the Plks.

In compound **11**, a 4-thiazole ring replaces the phenyl group of **9**. The compound maintained the same potency against Plk-2, but had an eightfold improvement in isoform selectivity (Table 2). The crystal structure of Plk-2–**11** (Figure 2d) shows a close contact between the sulfur atom in the thiazole and the side chain His169 (3.7 Å). Plk-1 has Glu140 in the corresponding position. Presumably the thiazole ring of **11** undergoes more favorable interactions with the basic His169 in Plk-2 than Glu140 in Plk-1. Variation of the 8-cyclopentane ring (**8**–**17**, Table 2) yielded compounds with good potency and improved selectivity for Plk-2 over Plk-1. Decreasing the size of the 8-substitutent to isopropyl (**12**) and to cyclobutyl (**13**) retained biochemical potency and increased the isoform selectivity between the Plks compared with compounds **3** and **9**. Replacing the cyclopentane ring of **9** with a tetrahydrofuran-3-yl ring gave a pair of diastereomers, **14** and **15**.[26] Diastereomer **15** was selected for further diversification due to its excellent Plk-2 biochemical activity and Plk isoform selectivity. The 3-fluoro analogue **16** displayed in vitro potency and selectivity similar to **15**. However, 4-fluoro **17** represented a 200-fold improvement in isoform selectivity over **9**. Fluorination at the *para*-position of the 2-(phenyl)imidazole confers microsome stability on **17** relative to the *meta*-fluorophenyl isomer **16**. To estimate the selectivity of the tetrahydrofuran-3-yl analogues, the *meta*-fluorophenyl analogue **16** was characterized in the 35-kinase panel at 10 μM concentration (Supporting Information table 1). Compound **16** did not inhibit any of the non-Plk kinases by $>40\%$.

Cellular activity against phosphorylation of α-synuclein for many of these analogues was also determined in a Plk-2-expressing HEK293 cell line (Table 2). Given the concentration of ATP in the enzyme assay (100 μM), a shift of ~10-fold was expected. However, in some cases an attenuation in cellular potency by two orders of magnitude relative to the biochemical activity was observed, suggesting some additional factor is exerting an influence.

Microsomal stability of the compounds **8**–**17** was roughly inversely proportional to their lipophilicity, as indicated by clog*P* values. While compound **9** exhibited very good potency against Plk-2 relative to **8**, its nearly two-log-unit jump in clog*P* was reflected by its extremely poor microsomal stability across species. Altering the placement of the phenyl group attenuated potency (analogue **10**). Switching from a pendent cy-

Table 2. Enzyme inhibition data and Plk isoform selectivity ratios for compounds **8**–**17**.

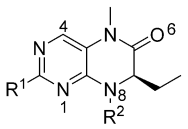

Compd	R^1	R^2	IC_{50} [μM][a] Plk-2	Plk-1	Plk-3	Selectivity Plk-2/Plk-1	EC_{50} [μM] HEK 293	MetStab (m,r,h)[b]	clog P[c]
8			0.56	4.24	–	7.6	–	39, 21, 66	3.4
9	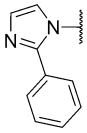		0.005	0.008	0.095	1.6	0.332	0, 0, 0	5.2
10	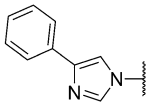		0.466	0.195	12.981	0.42	–	51, 5, 26	4.7
11	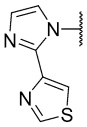		0.005	0.064	0.571	13	0.837	1, 0, 8	4.5
12	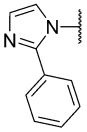		0.025	0.875	2.019	35	2.99	12, 0, 14	4.6
13	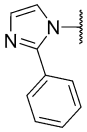		0.007	0.194	–	28	0.667	1, 0, 3	4.7
14	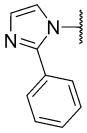		0.021	0.481	8.602	23	–	27, 0, 10	3.7
15	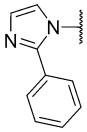		0.008	0.386	1.465	48	0.830	51, 13,17	3.7
16	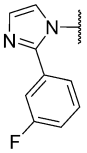		0.007	0.390	4.593	56	1.20	35, 1, 5	3.7
17	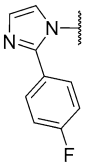		0.018	3.75	10.401	208	2.10	63, 67, 58	4.0

[a] Values are means of at least two experiments at 100 μM ATP concentration; details can be found in the Supporting Information. [b] See ref. [23]. [c] Details regarding the method of calculation can be found in the Supporting Information.

clopentyl ring at the 8-position of the pteridinone core to either a pendent isopropyl group, **12**, or cyclobutyl group, **13**, modestly improved the metabolic stability. With the exception of **11**, the addition of heteroatoms (**14**–**17**) and blocking potential metabolic oxidation sites (**16**, **17**) proved to be fruitful in generating stable analogues.

Metabolic identification studies in rat hepatocytes showed that **9** is extensively metabolized. The major sites of oxidative metabolism were shown to be the pendent cyclopentyl ring as well as the ethyl group, with demethylation accounting for only a small fraction of the total metabolites identified; depending on substitution, other analogues could suffer from metabolism on the biaryl group as well. A two-pronged strategy was employed to address this problem. Efforts were undertaken to overcome this undesired oxidative metabolism by lowering the log*P* of subsequent analogues and through directed heteroatom substitution. In the context of the bicyclic pteridine core, these focused efforts produced advanced analogues, one of which was used to generate promising evidence of target engagement in vivo.[19] However, our experience with methodical derivatization at the 8-position of the pteridinone ring compelled a more radical approach to variation of this sector. This was attempted by surveying analogues that kept the same basic architecture as **9**, but incorporated a fused cycloalkyl ring on the pteridinone core to provide 7,8-tricyclic pteridinone analogues (Figure 4).

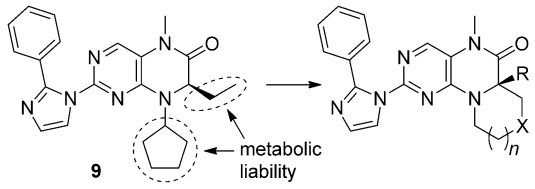

Figure 4. Increasing oxidative metabolic stability through cyclization and lowered log*P*.

Gratifyingly, lowering log*P* by fusing a ring to the pteridinone core did indeed improve stability toward oxidative metabolism, as shown in Table 3. Despite the approximate three-fold decrease in Plk-2 potency, there was also roughly a 100-fold improvement in Plk-2/Plk-1 selectivity of the 7,8-tricyclic pteridinone analogues relative to **9**. The exact reason for this has remained elusive. One possibility is that the tricyclic compounds undergo a more optimal edge-to-face interaction with Tyr161 of the hinge. An alternative explanation rests on the subtle changes in protein conformation that modulate the interaction of the P-loop with the inhibitors. Comparisons between published Plk-1 and our Plk-2 crystal structures indicate that Plk-2 has a wider gap between the N and C domains of the kinase. The shift in the N and C domains caused a 1–2 Å shift in the P-loop in the vicinity of the 8-substituent on the pteridinone ring. However, the pursuit of more detailed struc-

Table 3. Lowering log*P* improves oxidative metabolic stability in 7,8-tricyclic pteridinones.

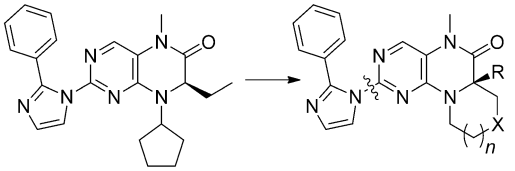

	Compound	IC_{50} [μM][a] Plk-2	Plk-1	Plk-3	Selectivity Plk-2/Plk-1	EC_{50} [μM] HEK293	log*P*	OxMet (m,r,h)[b]	Permeability [nm s^{-1}][b]	Solubility [μM][b]
18	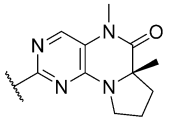	0.166	>10	–	60	–	1.9	76, 66, 88	243	100
19	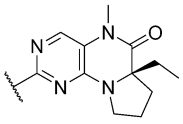	0.063	7.2	30.750	114	4.48	2.3	50, 75, 72	249	100
20	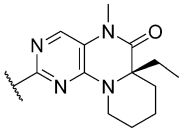	0.017	4.22	9.676	248	1.10	3.3	19, 2, 6	190	35
21	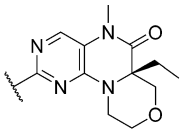	0.039	27.3	6.445	700	1.20	2.3	41, 60, 69	128	11
22	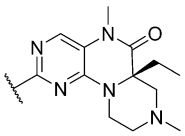	0.053	55.9	42.863	1054	4.70	2.3	50, 34, 49	–	6

[a] Values are means of at least two experiments at 100 μM ATP concentration; details can be found in the Supporting Information. [b] See ref. [23].

tural analyses would have required a direct comparison of Plk-2 and Plk-1 complexes with these compounds, and generation of the latter was outside of the scope of this effort.

Increasing ring size from the pyrrolidine **18** to the six-membered piperidine **20**, morpholine **21**, or piperazine **22** improved Plk-2 activity. Compound **19** illustrates the importance of the ethyl group for potency, as is evident by the 2.6-fold increase in potency relative to **18**. Despite its excellent potency and Plk-2/Plk-1 selectivity, with a measured log $P = 3.3$, compound **20** demonstrated only modest oxidative metabolic stability relative to **18** and **19**. Given the measured log P for **20**, it was not surprising to observe a decrease in aqueous solubility relative to **19**. Surprisingly, a dramatic decrease in solubility for **21** was observed, despite its lower measured log P, concomitant with a loss in permeability. Poor solubility notwithstanding, **21** offered the best combination of potency, oxidative metabolic stability, and Plk-2/Plk-1 and Plk-2/Plk-3 selectivity of the group. Compound **21** was evaluated in the kinase selectivity panel featuring 35 kinases (Supporting Information table 1) and an expanded selectivity panel of 303 kinases (Supporting Information table 2). It demonstrated excellent selectivity in both kinase panels: only MAP4K4 was inhibited at $>80\%$ at 10 μM concentration. The *N*-methyl replacement analogue **22**, compared with **21**, showed a modest loss in activity, both intrinsic and cellular, a modest loss in oxidative metabolic stability and solubility, but a 1.5-fold gain in Plk-2/Plk-1 selectivity.

Evaluation of the more potent analogues **19**–**22** in the cellular model showed that despite the lower measured log P values of these compounds, the cellular activity remained two orders of magnitude lower than the enzymatic activity. This was true despite excellent in vitro passive permeability throughout the series. Nevertheless, compound **21** emerged as the leading candidate with the best overall properties for further development.

To capitalize on the excellent kinome selectivity, potency, and oxidative stability demonstrated by **21**, a focused group of analogues with this advanced core was made by targeting A- and B-ring modifications, as shown in Figure 5. A-ring modifications were performed in an effort to increase Plk-2/Plk-1 selectivity, whereas B-ring modifications were explored in an effort to improve on the potency and physicochemical properties displayed by **21**.

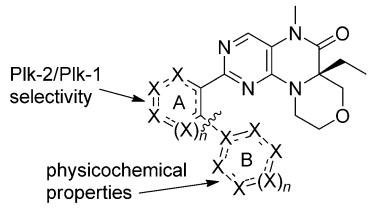

Figure 5. Modifications to the 7,8-tricyclic morpholine pteridines.

The A-ring replacements were examined in an attempt to increase Plk-2/Plk-1 selectivity, as well as to improve certain physicochemical properties such as solubility, oxidative stability, and permeability (Table 4). Pyridines as A-ring replacements provided little advantage over the imidazole found in **21**. Despite its favorable P-glycoprotein (P-gp) ratio, **23** fell short of the level of potency, Plk-2/Plk-1 selectivity, and oxidative metabolic stability displayed by **21**. Compound **24** exhibited potency similar to **21**, but it suffered from poorer selectivity and oxidative stability compared with **21**. Despite its low log P and excellent oxidative metabolic stability, triazole **25** showed a dramatic 250-fold loss in potency relative to **21** and a complete loss of Plk-2/Plk-1 selectivity. Indeed, the increased electron density proximal to Tyr161 may have induced a Coulombic repulsion, as evidenced by lower potency and selectivity. The isoxazole A-ring replacement **26** was also found to be suboptimal in all of the desired properties. Thiadiazole **27** was the most promising of the A-ring replacements that were examined, as it provided the greatest degree of Plk-2/Plk-1 selectivity, with potency and oxidative stability on par with that of **21**. Unfortunately, **27** proved insoluble under standard conditions. None of these analogues proved to be comparably potent in cell or enzyme activity to the previously synthesized inhibitors listed in Table 2.

The series of B-ring replacements brought mixed results with respect to the desired improvements over **21** in potency, Plk-2/Plk-1 selectivity, and physicochemical properties (Table 5). Compound **28** realized slight improvements in microsomal stability, solubility, and Plk-2/Plk-1 selectivity, but a slight loss in potency relative to **21**. Compound **29** displayed a twofold increase in potency over **21**, but a modest loss in Plk-2/Plk-1 selectivity. The B-ring of **30** was substituted with 4-fluoropyridylphenyl in an attempt to increase solubility. Despite the gain in microsomal stability, the solubility of **30** was the same as that of **21**, and the potency and Plk-2/Plk-1 selectivity were decreased by 9.5- and 2.5-fold, respectively. A similar increase in microsomal stability was observed for **31**, in addition to favorable solubility and permeability. However, the decrease in potency and selectivity were more pronounced, at 22.5- and 6-fold, respectively.

In vivo pharmacokinetic studies

Compounds **3**, **17**, and **21** were unique in these series because of their stability in the liver microsome assays, permeability, and potency against Plk-2. Each compound was examined in an in vivo model of brain exposure in mouse, as well as by obtaining the i.v./p.o. pharmacokinetic profiles in rat (Table 6). In the mouse brain uptake studies the rodents were given a 1 mg kg^{-1} i.v. bolus dose of either **3**, **17**, or **21**, and brain tissue and plasma were sampled at each time point. The results are reported as the AUC over a 3 h time course in both brain and plasma compartments and also expressed as a ratio of AUC values to give the brain to plasma (B/P) ratio. Compound **3** demonstrated excellent brain exposure in mouse; **21** showed lower but significant exposure, while **17** exhibited no significant brain exposure in mouse. The low brain exposure is consistent with the measured permeability for **17**. The efflux ratio both with and without the P-gp transport inhibitor tari-

Table 4. A-ring modifications affect Plk-2/Plk-1 selectivity.

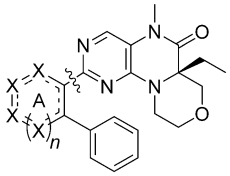

	Compound	IC_{50} [μM][a] Plk-2	Plk-1	Plk-3	Selectivity Plk-2/Plk-1	EC_{50} [μM] HEK293	log *P*	OxMet (m,r,h)[b]	Permeability [nm s^{-1}][b]	Solubility [μM][b]
23	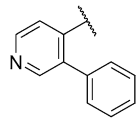	0.104	7.23	2.591	70	1.90	3.0	0, 25, 34	175	25
24	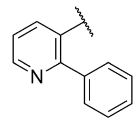	0.059	17.6	2.458	298	8.20	2.3	0, 37, 66	155	65
25	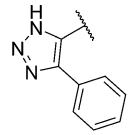	9.91	11.1	4.006	1	–	1.6	74, 87, 88	91	38
26	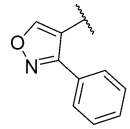	0.192	18.2	12.506	95	–	2.0	58, 6, 77	50	35
27	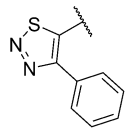	0.057	>100	4.966	1770	>10	–	45, 11, 52	126	0

[a] Values are means of at least two experiments at 100 mM ATP concentration; details can be found in the Supporting Information. [b] See ref. [23].

Table 5. B-ring substituent effects on potency and pharmacokinetics.

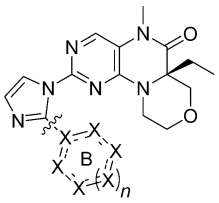

	Compound	IC_{50} [μM][a] Plk-2	Plk-1	Plk-3	Selectivity Plk-2/Plk-1	EC_{50} [μM] HEK293	log *P*	OxMet (m,r,h)[b]	Permeability [nm s^{-1}][b]	Solubility [μM][b]
28	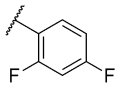	0.056	42.9	20.648	766	3.30	2.6	47, 67, 81	169	35
29	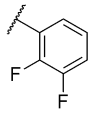	0.018	8.71	1.874	484	1.60	–	19, 33, 46	88	25
30	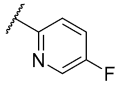	0.371	>100	53.022	270	–	3.3	59, 86, 91	164	11
31		0.879	>100	>100	114	–	1.6	77, 92, 96	213	100

[a] Values are means of at least two experiments at 100 mM ATP concentration; details can be found in the Supporting Information. [b] See ref. [23].

Table 6. In vivo PK parameters.

Compound:	3	17	21
Mouse brain uptake, 1 mg kg^{-1} i.v.			
plasma $AUC_{(0-3\,h)}$ [ng h^{-1} mL^{-1}]	205	2626	660
brain $AUC_{(0-3\,h)}$ [ng h^{-1} g^{-1}]	346	88	223
brain/plasma AUC ratio	1.7	0.03	0.3
Rat PK, 1 mg kg^{-1} i.v.			
$AUC_{(0-\infty)}$ [ng h^{-1} mL^{-1}]	123 ± 10	543 ± 82	449 ± 64
$t_{1/2}$ [h]	0.4 ± 0.2	0.5	1.5 ± 0.5
CL [mL h^{-1} kg^{-1}]	8191 ± 727	1871 ± 298	2256 ± 297
$Q_{hepatic}$ [%]	247	47	57
MRT [h]	0.4	0.5 ± 0.1	0.5 ± 0.1
V_{dss} [mL kg^{-1}]	3326 ± 128	922 ± 344	1164 ± 84
BW_{total} [%]	545	151	191
Rat PK, p.o.			
dose [mg kg^{-1}]	2	10	2
C_{max} [ng mL^{-1}]	60 ± 73	7593 ± 1696	1613 ± 478
t_{max} [h]	0.3 ± 0.1	0.25	0.25
$AUC_{(0-\infty)}$ [ng h^{-1} mL^{-1}]	32 ± 35	3729 ± 1029	1310 ± 916
$t_{1/2}$ [h]	0.3 ± 0.1	1.76 ± 0.15	0.8 ± 0.29
MRT [h]	0.6 ± 0.2	0.5	0.7 ± 0.2
F [%]	13	69	153

quidar present ($P_{eff(A-B)}/P_{eff(B-A)} = 27$) indicates that **17** is a moderate substrate for this transporter.

The rat i.v./p.o. pharmacokinetic profile for **3**, **17**, and **21** was reasonably consistent with the trends suggested by the in vitro ADME data. The poor microsomal stability in rat for **3** (16% of **3** remaining after a 30 min incubation) in addition to a possible extrahepatic metabolic pathway translated into large values for i.v. clearance (Table 6). Both **17** and **21** exhibited good stability in rat microsomes. Although the rates of clearance remained high, both **17** and **21** showed moderately improved rates of both absolute clearance and clearance relative to hepatic blood flow. All three compounds demonstrated excellent permeability in the in vitro MDCKII MDR-1 model. Good plasma exposures after oral administration and a high fraction of compound absorbed were observed for both **17** and **21**. However, the peripheral plasma exposures displayed by compound **17** were substantial. A 10 mg kg^{-1} single oral dose yielded an AUC of 3730 ng h^{-1} mL^{-1} with an oral $t_{1/2}$ of 1.76 h (Table 6), making **17** a suitable probe of the role of Plk-2 in the peripheral compartment rather than the CNS. The same parameters were considerably lower for **3**, consistent with the poor microsome stability and high i.v. clearance in rat. Based on the observed brain exposure and PK profile, **21** was advanced to an in vivo target engagement study in rat.

Target engagement

A CNS target engagement study confirmed the ability of **21** to cross the blood–brain barrier and achieve brain levels sufficient to inhibit the endogenous Plk-2-mediated phosphorylation of α-synuclein in rat brain. Administration of a single oral 100 or 200 mg kg^{-1} dose of **21** to Sprague–Dawley rats resulted in respective 34.5 and 41.4% decreases ($p < 0.0001$) in phospho-S129 α-synuclein levels in the cerebral cortex for up to 6 h (Figure 6a). The levels of total α-synuclein were unaffected by this treatment (Figure 6b). The brain-to-plasma ratios derived from the exposure data for **21** at 6 h following oral dosing in rats (Table 7) are in close agreement with the ratio predicted by the mouse brain uptake model (Table 6). The 6 h brain concentrations for **21** at the 100 and 200 mg kg^{-1} doses were respectively five- and sevenfold greater than the Plk-2 cellular IC_{50} value. As expected in vehicle-treated rats, total α-synuclein reached 60–70 mg g^{-1} with phospho-S129 α-synuclein representing only 0.1% of the total. In conclusion, compound **21** proved useful as a probe of Plk-2 in the CNS compartment, because it is not a P-gp substrate, and exhibits good permeability and high oral bioavailability. This compound was well tolerated in the target engagement study, and sustained 6.8 μM levels in the CNS up to 6 h after oral dosing in rat at 100 mg kg^{-1}.

Chemistry

The general synthetic route for the preparation of the various pteridinones listed in Tables 1 and 2 is illustrated in Scheme 1. Chloropteridinone intermedi-

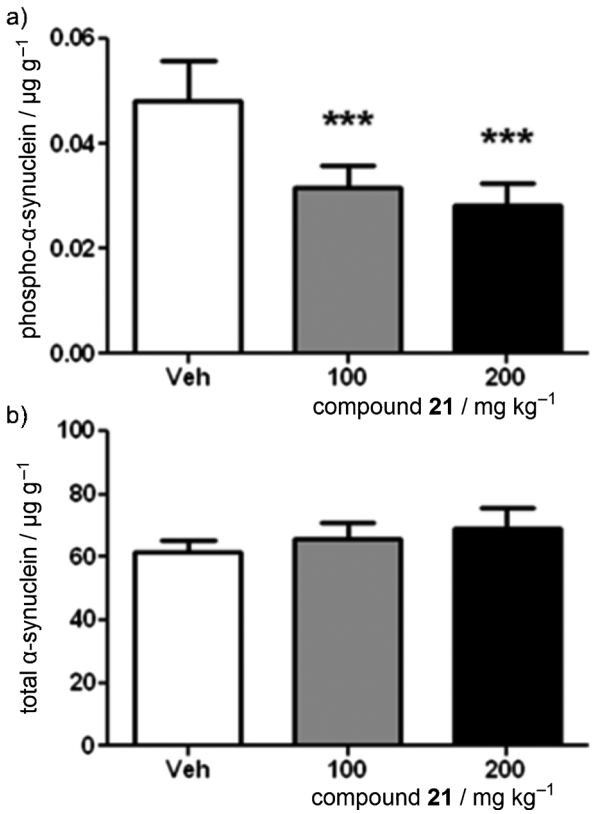

Figure 6. A single oral dose of **21** a) significantly decreases phospho-S129 α-synuclein levels in rat cerebral cortex, whereas b) total α-synuclein levels are unchanged. Data represent the mean ± SD with $n = 6$ for each group; the inhibition for each dose reaches significance (***$p < 0.0001$) versus vehicle control group (Veh) as determined by one-way ANOVA followed by Tukey's post hoc test.

Table 7. Mean plasma (P) and brain (B) levels of **21** at 6 h following a single oral dose.

Dose [mg kg^{-1}]	Time [h]	P [ng mL^{-1}]	B [ng g^{-1}]	B/P ratio
100	6	7756 ± 2032	2629 ± 1612	0.46
200	6	8141 ± 3556	3380 ± 1331	0.42

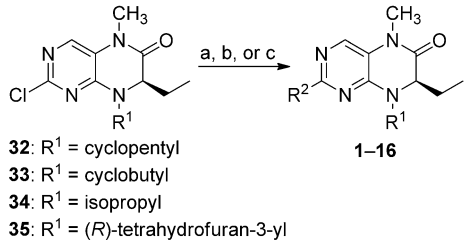

Scheme 1. General synthetic strategy. *Reagents and conditions*: a) N-heterocycle, Δ, Cs_2CO_3, DMF or DMSO; b) Ullmann coupling; c) Suzuki coupling.

ates **32**–**35** were prepared according to published procedures.[20] These intermediates could undergo heating with the appropriate N-heterocycle to provide the desired compounds. Alternatively, they could first be subjected to Ullmann or Suzuki coupling[27] to provide the desired compounds. The detailed syntheses of all compounds shown are described fully in the Supporting Information.

A representative synthesis of these 7,8-tricyclic pteridinone analogues is shown in Scheme 2. Each synthesis proceeded in a straightforward manner from the appropriate starting amino ester. The synthesis of **19** required the enantiopure amino ester **36**, derived in four steps from L-proline.[28] Reaction of amino ester **36** with 2,4-dichloro-5-nitropyrmidine (**37**) exclusively provided regioisomer **38**. Intramolecular iron-mediated reductive cyclization followed by methylation with trimethyl phosphate provided **39**, which could then be treated with 2-phenylimidazole to yield **19**.

In an analogous manner, the coupling of amine **40**[29] with excess 2,4-dichloropyrimidine gave an 8:1 mixture of the desired 4-substituted product **41** (67% yield) and the regioisomeric 2-substituted byproduct. Compound **41** was transformed into key intermediate **42** before displacement and chiral purification to afford final product **21**.

Advanced intermediate **42** provided a good point for diversification in the production of A-ring modifications, as shown in Scheme 3. Advanced intermediate **42** was partitioned down three divergent reaction paths. Suzuki reaction of **42** with the appropriate boronic acid (e.g., **43**) provided analogues **23**–**24** (Table 2). Sonogashira coupling of **42** with phenylacetylene followed by reaction with sodium azide afforded triazole **25**. The palladium-catalyzed reaction of **42** with acetophenone provid-

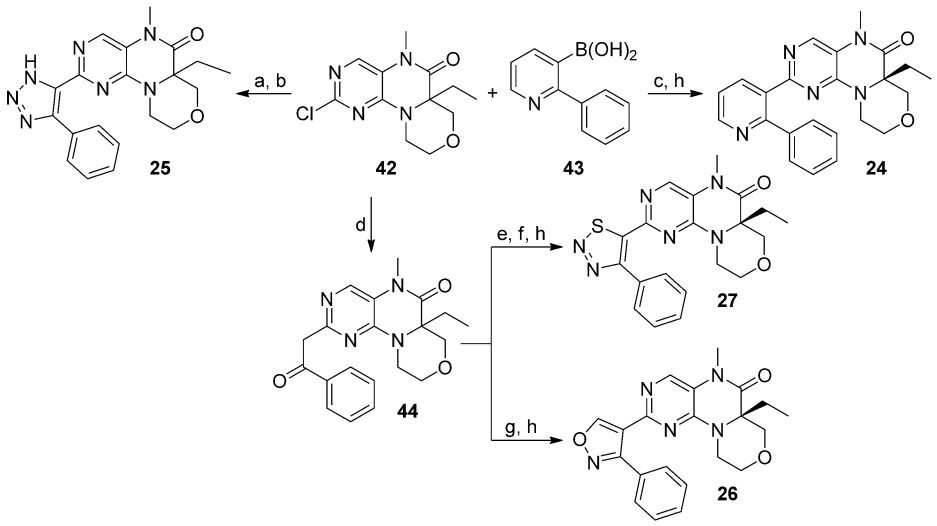

Scheme 3. A-ring modifications. *Reagents and conditions*: a) phenylacetylene, $Pd(PPh_3)_4$, CuI, Et_3N, CH_3CN, MW, 140 °C, 5 min; b) NaN_3, DMSO, MW, 120 °C, 1 h; c) Na_2CO_3, $Pd(dppf)Cl_2$, DME/H_2O, 90 °C; d) acetophenone, (1,3-bis(2,6-diisopropylphenyl)-4,5-dihydroimidazol-2-ylidene)Pd(Cl)allyl, *t*BuONa, THF, reflux; e) N_2H_4, EtOH, reflux, f) $SOCl_2$; g) DMF/DMA, DMF, AcOH, $NH_2OH{\cdot}HCl$; h) chiral HPLC.

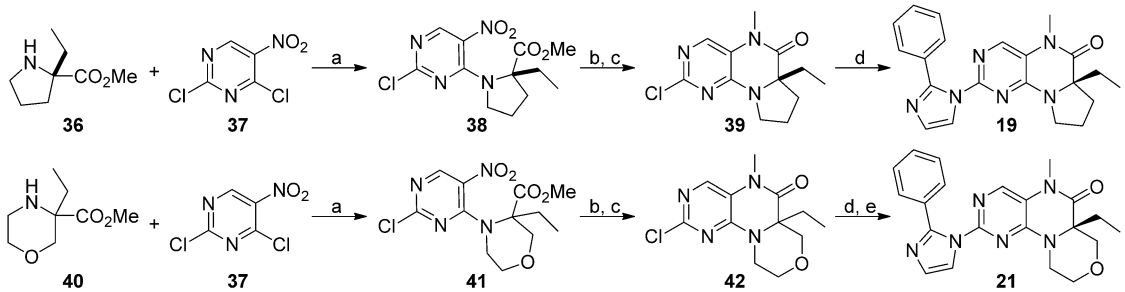

Scheme 2. Representative synthesis of the 7,8-tricyclic pteridinone analogues. *Reagents and conditions*: a) DIPEA, THF, 0 °C; b) Fe, AcOH, 90 °C; c) $(CH_3)_3PO_4$, K_2CO_3, dioxane, 90 °C; d) 2-phenylimidazole, Na_2CO_3, DMF, 150 °C; e) chiral HPLC.

ed advanced intermediate **44**, which could either be treated with DMF/DMA and hydroxylamine to afford **26**, or with hydrazine and thionyl chloride to give **27**.

Conclusions

These efforts resulted in novel, potent, and selective inhibitors of Plk-2, with pharmaceutical properties sufficient to enable successful in vivo target-engagement studies with compound **21**. The now commonly used structure-guided discovery approach to engineer a ligand-efficient core for increased potency and selectivity by crystallographic and computational means provided a powerful framework for these compounds to be designed and synthesized in an efficient manner. By altering the design of the hinge region interface of the molecules to use a tandem hydrogen bond/aromatic edge-to-face interaction and effectively exploiting the space between Tyr161 and Arg165, the overall selectivity of these analogues versus non-Plk kinases was significantly enhanced. Incorporating a fused ring into the pteridine core further enhanced both selectivity and pharmaceutical properties, and gave rise to key compound **21**.

Compound **21** is a useful tool for understanding the consequence of inhibiting Plk-2 on synuclein phosphorylation in rat brain. Continuing focus is placed on confirming the hypothesis that α-synuclein phosphorylation is a key step in the pathophysiology of Parkinson-like symptoms.[30] The proof-of-principle studies in a rodent model of transgenic[31] or virally induced synuclein overexpression[32] will require a well-tolerated agent capable of suppressing synuclein phosphorylation in the CNS compartment over a sustained period of time. Compound **21** was identified as a compound that is highly selective for the target and achieved the concentrations required in vivo to effectively inhibit synuclein phosphorylation by Plk-2 in wild-type rat brain. Further studies are required to define the effect of repeated oral dosing on α-synuclein phosphorylation in rodent brain.

Experimental Section

X-ray crystallography

Crystallization: Plk-2 kinase domain A2 mutant protein at 8 mg mL^{-1} in buffer (final buffer) was incubated on ice with 1 mM staurosporine for 30 min. The drops were set up with a 1:1 (*v*/*v*) ratio of protein to mother liquor in a total volume of 2 μL. Diffraction-quality crystals of Plk-2 kinase domain in complex with the compound were obtained by the sitting-drop vapor diffusion method at 277 K against a reservoir containing 0.1 M Bis-Tris pH 5.5, 0.8 M sodium formate, 19% PEG 3350. Crystals appeared in 2–3 days and developed to full size in 2–3 weeks. Crystals were mounted directly from the drops and flash-frozen in liquid nitrogen. Apo-crystals can be obtained under the same conditions described above, except that a low-affinity small fragment compound was added at 1 mM concentration in an attempt to obtain co-crystals with this compound. The crystal structure showed the compound to be absent.

Data collection and structure determination: Diffraction data were collected on beamline 5.0.2 at ALS and were processed using HKL-2000.[33] The first Plk-2 structure was determined by molecular replacement using Plk-1 (PDB code 2RKU) as a searching model with the ligand and water molecules removed. The subsequent rounds of manual model building and TLS refinement were performed using Coot[34] and Refmac 5, respectively.[35] PDB entry designations for Plk-2 complexes with compounds **1**, **1a**, **4**, **9**, and **11** are shown in the legends of Figures 1 and 2.

Molecular dynamics simulations

Compound synthesis was guided by computer simulation. Each candidate for chemical synthesis was evaluated for its potential binding affinity to the protein using the molecular mechanics Poisson–Boltzmann surface area (MM-PBSA) methodology as implemented in the AMBER 10 molecular simulation program suite.[36] Compounds with higher predicted affinities were prioritized for synthesis.

The MM-PBSA method calculates protein–ligand binding affinity by taking the average interaction and solvation energies over a set of conformations obtained from a room-temperature molecular dynamics (MD) simulation of the solvated protein–ligand complex. The protocol to obtain this set of complex structures is as follows: The ligand to be evaluated was constructed by in situ modification of protein–ligand complex (obtained from X-ray crystallography) using the Maestro molecular modeling package (Schrödinger, Inc.). MD parameters for the ligand were obtained from the ANTECHAMBER module.[37] AMBER's solvateCap feature was used to add water molecules to a sphere of 29 Å radius centered on the ligand. Protein atoms on residues with α-carbons 15 Å beyond all ligands atom were frozen during the simulation.

This initial structure was equilibrated to a room-temperature production MD run in eight sequential steps (Table 8). The conformations of the solvated protein–ligand complex were sampled at 1 ps intervals in the production MD run (Step 8 in Table 8). Binding free energies were computed for each sampled conformation and averaged over the 250 samples to obtain the estimated affinity for the ligand. Replicate simulations were conducted by using slightly varied starting coordinates (1% of coordinates randomly perturbed by ±0.001 Å). Eight replicate simulations using the protocol in Table 8 were then averaged to obtain the final estimate of ligand binding energy.

Selectivity panel of single-point kinase inhibition data

The kinase profiling panel used, SelectScreen, is provided as a commercial service by InVitrogen/Life Technologies (Grand Island, NY, USA). Compounds were tested at a concentration of 10 μM, while the ATP concentration used in these assays was $2\times K_M$; the assays are a mixture of formats: Z′-LYTE, Adapta, and LanthaScreen technologies.

In vivo studies

All animal use procedures were approved by the Institutional Animal Care and Use Committee (IACUC) at Elan Pharmaceuticals and performed in accordance with the National Research Council Guide for the Care and Use of Laboratory Animals (Institute of Laboratory Animal Resources, National Research Council, 1996), and all applicable regulations.

Table 8. MD protocol for the MM/PBSA estimation of binding energies.

Step	Description	Convergence Criterion or Duration[a]	Constrained Atoms	Magnitude of Restraint [kcal mol^{-1} Å^{-1}]	T [K][b]
1	Minimization: water H atoms	0.01 RMSD	All protein and ligand atoms and water molecule oxygen atoms	10.0	–
2	Minimization: water molecules	0.01 RMSD	All protein and ligand atoms	4.0	–
3	Dynamics: water molecules	25 ps	All protein and ligand atoms	4.0	0–200
4	Minimization: ligand and water molecules	0.01 RMSD	All protein atoms	1.5	–
5	Minimization: entire system	0.01 RMSD	Protein α-carbon atoms	1.5	–
6	Dynamics: raise temperature	50 ps	Protein α-carbon atoms	1.5	0–300
7	Dynamics: equilibration	100 ps	Protein α-carbon atoms	1.5	300
8	Dynamics: production run	250 ps	Protein α-carbon atoms	1.5	300

[a] For minimization steps, the RMSD convergence criterion is listed; for dynamics steps, the time of the simulation is listed. [b] For temperature ranges, the temperature was linearly scaled over the time interval of the simulation.

Pharmacokinetics assays

Two- to three-month old female FVB mice were obtained from Taconic Farms (Hudson, NY, USA), and male jugular-vein-cannulated Sprague–Dawley rats (approximately 8 weeks of age) were obtained from Charles River Laboratories (Hollister, CA, USA).

Mouse brain uptake assay: Test compounds were formulated for i.v. dosing in a vehicle containing 5% Solutol/10% propylene glycol in saline on the day of dosing. Compounds were formulated at a concentration of 0.2 mg mL^{-1} and administered via tail vein bolus at a dosage of 1 mg kg^{-1}. Samples were collected (three mice per time point) at 0.083, 0.5, 1, 3, and 6 h post-dose. Blood samples, collected by cardiac puncture, were transferred to tubes containing tripotassium EDTA and stored on ice prior to centrifugation. Samples were centrifuged at 10000 rpm at 4 °C for 5 min to obtain plasma. Dissected brain samples (right hemisphere) were rinsed, weighed, and immediately frozen with dry ice. All samples were stored at −80 °C prior to bioanalysis.

Rat pharmacokinetic assay: Rats received either a 1 mg kg^{-1} intravenous bolus ($n=3$) or a 2 mg kg^{-1} oral gavage dose of test article. Test articles for intravenous (i.v.) administration were formulated as solutions in Solutol/propylene glycol/water (10:20:70% *v/v/v*) for sterile injection. The dose volume for i.v. administration was 1 mL kg^{-1}. Oral doses were formulated as suspensions in 0.5% Tween 80 in 2% methylcellulose at a dose volume of 5 mL kg^{-1}. Animals receiving oral doses were fasted overnight and for 4 h after dosing. Following test article administration, serial blood samples at 0.083 (i.v. only), 0.25, 0.5, 1, 2, 4, 6, 8, 12, and 24 h into K_3EDTA vials. Samples were transferred to tubes containing tripotassium EDTA and stored on ice prior to centrifugation. Samples were centrifuged at 10000 rpm at 4 °C for 5 min to obtain plasma. All samples were stored at −80 °C prior to bioanalysis.

Bioanalysis: Prior to analysis, brain tissue was homogenized with five parts 50 mM ammonium acetate buffer (pH 7.4). Test article concentrations in rat and mouse plasma and mouse brain homogenate samples were analyzed by using an LC–MS–MS method. Samples were prepared by protein precipitation using CH_3CN (with internal standard). Following mixing and centrifugation the supernatant was injected into the LC–MS–MS system. The LC–MS–MS system was composed of an Agilent 1290 LC HPLC system (Santa Clara, CA, USA), a CTC HTC Autosampler (Leap Technologies, Carrborro, NC, USA) and an ACE 2.1×50 mm C_{18} 1.8 μm LC column (MacMOD Analytical Inc. Chadds Ford, PA, USA). Separation was achieved using a 2.5 min gradient at a flow rate of 0.6 mL min^{-1}. Multi-reaction monitoring was used to detect the analytes of interest. Data acquisition and analysis was conducted using Analyst version 1.5.1.

Pharmacokinetic analysis: For mice mean composite plasma concentration–time and brain concentration–time profiles were generated for each test article. Non-compartmental pharmacokinetic analysis using the composite profiles was conducted using WinNonlin Professional Version 5.2 (Pharsight, Mountain View, CA, USA). Individual rat plasma profiles following i.v. and p.o. dosing were used to calculate pharmacokinetic parameters. Parameters determined include, as applicable, area under the plasma concentration–time profile ($AUC_{(0-\infty)}$), the terminal half-life ($t_{1/2}$), clearance (CL), volume of distribution at steady-state (V_{dss}), time to maximum concentration (t_{max}), and maximum concentration (C_{max}). The ratio of brain concentration to plasma concentration (B/P ratio) was calculated using $AUC_{(0-\infty)}$ values and individual time points. Oral bioavailability was calculated at the ratio of the dose-normalized $AUC_{(0-)}$ following p.o. dosing and $AUC_{(0-)}$ following i.v. dosing. Summary statistics were calculated using MS Excel, MS Office 2003 (Redmond, WA, USA).

Target engagement study: inhibition of Plk-2 phosphorylation of α-synuclein in rat brain

Dosing and tissue collection: Male Sprague–Dawley rats (Charles River, Gilroy, CA, USA) weighing ~100–120 g were given compound **20** orally (in 5% DMSO in 1% methylcellulose, volume: 10 mL kg^{-1}) as a single dose of either 100 or 200 mg kg^{-1} ($n=6$ per group). Rats were euthanized by CO_2 narcosis 6 h after dosing, and brains were removed quickly; the cerebral cortex was dissected out, placed on ice, and frozen at −80 °C until quantification of total and phosphorylated α-synuclein by ELISA.

Quantification of α-synuclein levels by ELISA: Because Plk-2 has been proposed as the main enzyme responsible for α-synuclein phosphorylation at serine 129,[3,4] we monitor the changes in phospho-S129 α-synuclein levels as a measure of Plk-2 activity in the brain. The total α-synuclein and phospho-S129 α-synuclein levels were quantified with a sandwich ELISA as described previously[2c,3] with some modifications.

Brain samples were homogenized with a bead-based Qiagen Tissuelyzer in 0.4% CHAPS solution containing phosphatase and protease inhibitors. The resulting homogenate was centrifuged at 14000 *g* for 20 min in an Eppendorf microcentrifuge. The supernatant CHAPS-soluble fraction was removed and diluted 1:20 with cell extraction buffer consisting of 0.1% SDS, 0.5% deoxycholate,

1% Triton X-100 and phosphatase inhibitors at a final concentration of 20%. For the detection of total α-synuclein, the monoclonal antibody 1H7 (amino acids 91–99) was used as the capture antibody and the biotinylated 5C12 antibody (amino acids 109–120) as the reporter antibody. For the detection of phospho-S129 α-synuclein levels, 1H7 was used as the capture antibody and biotinylated 11A5 (amino acids 124–134, specific to S129 phosphorylation) as the reporter antibody. The detection limit for phospho-S129 α-synuclein was 0.005 $\mu g\,g^{-1}$.

Representative synthetic procedures and exemplified analogues

Reagents and solvents obtained from commercial suppliers were used without further purification unless otherwise stated. Imidazole precursors for inhibitors **28**–**31** were synthesized by published methods.[38] Thin-layer chromatography was performed on precoated 0.25 mm silica gel plates (E. Merck, silica gel 60 F_{254}). Visualization was achieved using UV illumination or by staining with phosphomolybdic acid, ninhydrin, or other common staining reagents. Flash chromatography was performed with either a Biotage Flash 40 system and pre-packed silica gel columns or hand-packed columns (E. Merck silica gel 60, 230–400 mesh). Preparatory HPLC was performed on a Varian Prepstar high-performance liquid chromatograph. All final compounds were obtained in $\geq$95% purity. ^{1}H and ^{13}C NMR spectra were recorded at 300, 400, or 500 MHz and 75, 100 or 125 MHz, respectively, on a Varian Gemini or Bruker Avance spectrometer. Chemical shifts (δ) are reported in parts per million downfield relative to tetramethylsilane or to proton resonances resulting from incomplete deuteration of the NMR solvent. Mass spectra were recorded on an Agilent series 1100 mass spectrometer connected to an Agilent series 1100 HPLC. Elemental analyses were performed at ALS Environmental (Tucson, AZ, USA).

LC–MS and HRMS analysis on a Q-TOFMS: Stock solutions (20 mM) for all standard compounds prepared in DMSO were diluted in water to 5 μM for positive-mode mass spectrometric analysis. This typically produced maximum ion abundances on the order of 1×10^6–5×10^6 ions per scan, although for data processing, spectra with ion abundances of 5×10^5 ions/scan were averaged. A triple-TOF 5600 quadrupole time-of-flight hybrid mass spectrometer (AB Sciex, Foster City, CA, USA) equipped with an LC system consisting of a LEAP PAL HTC autosampler and an Agilent 1290 Infinity LC pump (Agilent, Santa Clara, CA, USA), was used for LC–MS analysis. The mass spectrometer was operated in the positive ionization mode with a spray voltage of 5.5 kV. Ion source gas 1, ion gas source 2, and curtain gas were set at 40, 45, 250 psi, respectively; the source temperature was maintained at 500 °C. Samples (5 μL) were introduced to the mass spectrometer via the HPLC system using an Agilent EC-C_{18} column (2.1×75 mm, 2.7 μm) under isocratic conditions (50:50 CH_3CN/H_2O with 0.1% formic acid) at a flow rate of 0.8 $mL\,min^{-1}$.

Full-scan mass spectra were acquired over the range of 120–900 *m/z* with an accumulation time of 0.25 s. Total acquisition time was 2 min per sample, and all four time-to-digital converter channels were used for detection. The tripleTOF instrument was calibrated by an integrated calibration delivery system (AB Sciex) using the manufacturer's positive calibration solution, at an injection flow rate of 300 $\mu L\,min^{-1}$. These calibrant ions were introduced via an orthogonal atmospheric pressure chemical ionization source in the presence of mobile phase flow. Mass spectral data acquisition and processing were performed using Analyst TF 1.5 and Peak View 1.1.1.2 software.

Reversed-phase HPLC methods

Analytical method A: The initial solvent composition was 20% CH_3CN with 0.1% trifluoroacetic acid (TFA) and H_2O with 0.1% TFA which ramped to 70% CH_3CN over 10 min, held at 70% for 2 min, then ramped to 95% over 1 min, and held at 95% for 2 min with a flow rate of 1.5 $mL\,min^{-1}$ at 35 °C.

Analytical method B: The same parameters as Method A changed so that the initial solvent composition was 50% CH_3CN which ramped to 95% CH_3CN over 10 min with a flow rate of 1.5 $mL\,min^{-1}$, at 35 °C.

Analytical method C: The same parameters as Method A changed so that the initial solvent composition was 20% CH_3CN which ramped to 50% CH_3CN over 10 min with a flow rate of 1.5 $mL\,min^{-1}$, at 35 °C.

Analytical method D: The same parameters as Method A changed so that the initial solvent composition was 5% CH_3CN which ramped to 20% CH_3CN over 10 min with a flow rate of 1.5 $mL\,min^{-1}$, at 35 °C.

Analytical method E: Solvent A: H_2O (0.05% TFA), solvent B: CH_3CN (0.05% TFA); gradient: 5→95% B in 1.4 min; flow rate: 2.3 $mL\,min^{-1}$; column: SunFire C_{18}, 4.6×50 mm, 3.5 μm; oven temperature: 50 °C.

Analytical Method F: Mobile phase A: H_2O (0.01% NH_3), phase B: CH_3CN; gradient: 5→95% B in 1.6 min; flow rate: 1.8 $mL\,min^{-1}$; column: XBridge C_{18}, 4.6×50 mm, 3.5 μm; oven temperature: 40 °C.

(*R*)-8-Cyclopentyl-7-ethyl-5-methyl-7,8-dihydropteridin-6(5*H*)-one (1 a): ^{1}H NMR (500 MHz, $CDCl_3$): δ=8.28 (s, 1H), 7.79 (s, 1H), 4.45–4.35 (m, 1H), 4.17 (dd, *J*=7.8, 3.8 Hz, 1H), 3.27 (s, 3H), 2.05–1.95 (m, 1H), 1.95–1.85 (m, 1H), 1.85–1.70 (m, 4H), 1.70–1.50 (m, 3H), 0.78 ppm (t, *J*=7.5 Hz, 3H); LC–MS *m/z*: 261.0 $[M+H]^+$; t_R=1.37 min (Method E); HRMS (ESI+) *m/z* calcd for $C_{14}H_{21}N_4O^+$ 261.1710, found 261.1710.

(*R*)-8-Cyclopentyl-7-ethyl-5-methyl-2-(pyrrolidin-1-yl)-7,8-dihydropteridin-6(5*H*)-one (2): ^{1}H NMR (400 MHz, $CDCl_3$): δ=7.61 (s, 1H), 4.20 (t, *J*=8.0 Hz, 1H), 4.15 (q, *J*=3.6 Hz, 1H), 3.60–3.48 (m, 4H), 3.28 (s, 3H), 2.20–1.90 (m, 7H), 1.90–1.75 (m, 4H), 1.75–1.55 (m, 3H), 0.86 ppm (t, *J*=7.6 Hz, 3H); LC–MS *m/z*: 330.0 $[M+H]^+$; t_R=1.52 min (Method E); HRMS (ESI+) *m/z* calcd for $C_{18}H_{28}N_5O^+$ 330.2288, found 330.2291.

(*R*)-8-Cyclopentyl-7-ethyl-2-(1*H*-imidazol-1-yl)-5-methyl-7,8-dihydropteridin-6(5*H*)-one (3): ^{1}H NMR (500 MHz, $CDCl_3$): δ=8.50 (s, 1H), 7.78 (s, 1H), 7.76 (s, 1H), 7.14 (s, 1H), 4.33–4.26 (m, 2H), 3.37 (s, 3H), 2.17–2.10 (m, 1H), 2.05–1.82 (m, 6H), 1.80–1.67 (m, 3H), 0.88 ppm (t, *J*=7.5 Hz, 3H); LC–MS (0.01% NH_3) *m/z*: 327.2 $[M+H]^+$; t_R=1.97 min (Method F); Anal. calcd for $C_{17}H_{22}N_6O$: C 62.56, H 6.79, N 25.75, found C 62.38, H 6.91, N 25.55.

(*R*)-8-Cyclopentyl-7-ethyl-5-methyl-2-(1*H*-pyrrol-2-yl)-7,8-dihydropteridin-6(5*H*)-one (4): ^{1}H NMR (500 MHz, $CDCl_3$): δ=9.66 (br s, 1H), 7.81 (s, 1H), 6.96 (s, 1H), 6.90 (s, 1H), 6.30 (d, *J*=2.5 Hz, 1H), 4.38 (pent, *J*=8.3 Hz, 1H), 4.25 (dd, *J*=8.0, 3.5 Hz, 1H), 3.34 (s, 3H), 2.15–2.05 (m, 1H), 2.05–1.92 (m, 2H), 1.92–1.80 (m, 4H), 1.77–1.60 (m, 3H), 0.86 ppm (t, *J*=7.3 Hz, 3H); LC–MS *m/z*: 326.0 $[M+H]^+$; t_R=1.54 min (Method E); HRMS (ESI+) *m/z* calcd for $C_{18}H_{24}N_5O^+$ 326.1975, found 326.1978.

(*R*)-8-Cyclopentyl-7-ethyl-5-methyl-2-(1*H*-pyrazol-4-yl)-7,8-dihydropteridin-6(5*H*)-one (5): ^{1}H NMR (500 MHz, $CDCl_3$): δ=8.26 (br s, 2H), 7.86 (s, 1H), 4.37 (t, *J*=8.3 Hz, 1H), 4.30–4.25 (m, 1H), 3.35 (s, 3H), 2.15–2.05 (m, 1H), 2.05–1.95 (m, 2H), 1.95–1.80 (m, 4H), 1.80–

1.65 (m, 3H), 0.87 ppm (t, $J=7.3$ Hz, 3H); LC–MS m/z: 327.0 $[M+H]^+$; $t_R=1.42$ min (Method E); HRMS (ESI+) m/z calcd for $C_{17}H_{23}N_6O^+$ 327.1928, found 327.1929.

(*R*)-8-Cyclopentyl-7-ethyl-5-methyl-2-(thiazol-5-yl)-7,8-dihydropteridin-6(5*H*)-one (6): ^{1}H NMR (500 MHz, CD_3OD): $\delta=9.03$ (s, 1H), 8.50 (s, 1H), 7.98 (s, 1H), 4.38 (dd, $J=7.5$, 3.5 Hz, 1H), 4.30 (pent, $J=8.5$ Hz, 1H), 3.40 (s, 3H), 2.25–2.15 (m, 1H), 2.15–1.90 (m, 6H), 1.90–1.80 (m, 1H), 1.80–1.65 (m, 2H), 0.85 ppm (t, $J=7.5$ Hz, 3H); LC–MS m/z: 344.1 $[M+H]^+$; $t_R=2.108$ min (Method F); HRMS (ESI+) m/z calcd for $C_{17}H_{22}N_5OS^+$ 344.1540, found 344.1543.

(*R*)-8-Cyclopentyl-7-ethyl-5-methyl-2-(pyridin-4-yl)-7,8-dihydropteridin-6(5*H*)-one (7): ^{1}H NMR (500 MHz, $CDCl_3$): $\delta=8.72$ (d, $J=4.5$ Hz, 2H), 8.17 (d, $J=4.5$ Hz, 2H), 7.99 (s, 1H), 4.46 (pent, $J=8.5$ Hz, 1H), 4.32 (dd, $J=7.8$, 3.8 Hz, 1H), 3.40 (s, 3H), 2.23–2.10 (m, 1H), 2.10–1.95 (m, 2H), 1.95–1.80 (m, 4H), 1.80–1.65 (m, 3H), 0.88 ppm (t, $J=7.5$ Hz, 3H); LC–MS (0.05% TFA) m/z: 338.0 $[M+H]^+$; $t_R=1.47$ min (Method E); HRMS (ESI+) m/z calcd for $C_{19}H_{24}N_5O^+$ 338.1975, found 338.1978.

(*R*)-8-Cyclopentyl-7-ethyl-5-methyl-2-(2-methyl-1*H*-imidazol-1-yl)-7,8-dihydropteridin-6(5*H*)-one (8): ^{1}H NMR (400 MHz, $CDCl_3$): $\delta=7.89$ (d, $J=2.0$ Hz, 1H), 7.83 (s, 1H), 7.33 (d, $J=2.0$ Hz, 1H), 4.42 (t, $J=8.0$ Hz, 1H), 4.36 (q, $J=3.7$ Hz, 1H), 3.41 (s, 3H), 3.10 (s, 3H), 2.21–2.08 (br s, 1H), 2.08–1.62 (m, 9H), 0.90 ppm (t, $J=7.5$ Hz, 3H); ^{13}C NMR (100 MHz, $CDCl_3$): $\delta=163.5$, 152.2, 148.5, 145.6, 136.4, 121.9, 119.3, 118.8, 60.1, 59.4, 29.4, 29.0, 28.4, 27.6, 23.5, 23.2, 14.9, 8.9 ppm; LC–MS m/z: 341.2 $[M+H]^+$; $t_R=6.16$ min (Method A); HRMS (ESI+) m/z calcd for $C_{18}H_{25}N_6O^+$ 341.2084, found 341.2093.

(*R*)-8-Cyclopentyl-7-ethyl-5-methyl-2-(2-phenyl-1*H*-imidazol-1-yl)-7,8-dihydropteridin-6(5*H*)-one (9): ^{1}H NMR (400 MHz, $CDCl_3$): $\delta=7.79$ (s, 1H), 7.75 (d, $J=1.2$ Hz, 1H), 7.65–7.40 (m, 6H), 4.22 (q, $J=3.6$ Hz, 1H), 3.61 (t, $J=8.1$ Hz, 1H), 3.38 (s, 3H), 1.95–1.80 (m, 1H), 1.70–1.50 (m, 5H), 1.50–1.20 (m, 4H), 0.81 ppm (t, $J=7.5$ Hz, 3H); LC–MS m/z: 403.2 $[M+H]^+$; $t_R=7.33$ min (Method C); HRMS (ESI+) m/z calcd for $C_{23}H_{27}N_6O^+$ 403.2241, found 403.2247.

(*R*)-8-Cyclopentyl-7-ethyl-5-methyl-2-(4-phenyl-1*H*-imidazol-1-yl)-7,8-dihydropteridin-6(5*H*)-one (10): ^{1}H NMR (400 MHz, $CDCl_3$): $\delta=9.34$ (s, 1H), 8.15 (s, 1H), 7.79–7.83 (m, 3H), 7.42–7.53 (m, 3H), 4.40–4.48 (m, 1H), 4.34–4.36 (m, 1H), 3.41 (s, 3H), 1.79–2.20 (m, 10H), 0.95 ppm (t, $J=7.3$ Hz, 3H); LC–MS m/z: 403.1 $[M+H]^+$; $t_R=5.049$ min (Method A).

(*R*)-8-Cyclopentyl-7-ethyl-5-methyl-2-(2-(thiazol-4-yl)-1*H*-imidazol-1-yl)-7,8-dihydropteridin-6(5*H*)-one (11): ^{1}H NMR (400 MHz, $CDCl_3$): $\delta=8.72$ (s, 1H), 8.58 (s, 1H), 7.81 (s, 1H), 7.68 (s, 1H), 7.48 (s, 1H), 4.28 (dd, $J=7.4$, 3.4 Hz, 1H), 3.85 (m, 1H), 3.42 (s, 3H), 1.47–1.94 (m, 10H), 0.90 ppm (t, $J=7.4$ Hz, 3H); LC–MS m/z: 410.1 $[M+H]^+$; $t_R=5.353$ min (Method C).

(*R*)-7-Ethyl-8-isopropyl-5-methyl-2-(2-phenyl-1*H*-imidazol-1-yl)-7,8-dihydropteridin-6(5*H*)-one (12): A mixture of intermediate **34** (100 mg, 0.37 mmol), 2-phenyl-1*H*-imidazole (533 mg, 3.7 mmol), Cu^I (35 mg, 0.18 mmol), *trans*-1,2-bis(methylamino)cyclocyclohexane (52.5 mg, 0.07 mL, 0.37 mmol) and solid K_2CO_3 (511 mg, 3.7 mmol) in 2 mL DMF was heated in a microwave reaction apparatus for 2 h at 200 °C. After this time the reaction was transferred to a round-bottom flask with the aid of EtOAc, then evaporated. The residue was purified by reversed-phase (RP) HPLC (PLRPS C_{18} column, eluting with a gradient of 20–25% CH_3CN in H_2O over 30 min) to give the title compound. ^{1}H NMR (400 MHz, $CDCl_3$): $\delta=7.81$ (d, $J=2.0$ Hz, 1H), 7.78 (s, 1H), 7.61 (d, $J=2.0$ Hz, 1H), 7.50 (m, 5H), 4.29 (dd, $J=7.2$, 3.2 Hz, 1H), 3.74 (m, 1H), 3.37 (s, 3H), 1.92 (m, 1H), 1.65 (m, 1H), 1.05 (d, $J=6.8$ Hz, 3H), 0.88 (d, $J=6.8$ Hz, 3H), 0.80 ppm (t, $J=7.6$ Hz, 3H); LC–MS m/z: 377.2 $[M+H]^+$; $t_R=4.065$ min (Method C); HRMS (ESI+) m/z calcd for $C_{21}H_{25}N_6O^+$ 377.2084, found 377.2088.

(*R*)-8-Cyclobutyl-7-ethyl-5-methyl-2-(2-phenyl-1*H*-imidazol-1-yl)-7,8-dihydropteridin-6(5*H*)-one (13): ^{1}H NMR (300 MHz, $CDCl_3$): $\delta=7.78$–7.76 (m, 2H), 7.62–7.60 (m, 1H), 7.57–7.50 (m, 3H), 7.49–7.43 (m, 2H), 4.27–4.24 (m, 1H), 3.69–3.57 (m, 1H), 3.37 (s, 3H), 1.98–1.40 (m, 8H), 0.78 ppm (t, $J=7.5$ Hz, 3H); LC–MS m/z: 389.2 $[M+H]^+$; $t_R=6.59$ min (Method C); HRMS (ESI+) m/z calcd for $C_{22}H_{25}N_6O^+$ 389.2084, found 389.2088.

(*R*)-7-Ethyl-5-methyl-2-(2-phenyl-1*H*-imidazol-1-yl)-8-((*S*)-tetrahydrofuran-3-yl)-7,8-dihydropteridin-6(5*H*)-one (14): ^{1}H NMR (400 MHz, $CDCl_3$): $\delta=7.84$ (m, 2H), 7.45–7.62 (m, 6H), 4.30 (dd, $J=7.1$, 2.6 Hz, 1H), 3.88–3.94 (m, 2H), 3.55–3.59 (m, 2H), 3.42–3.48 (m, 1H), 3.38 (s, 3H), 1.61–1.91 (m, 4H), 0.82 ppm (t, $J=7.5$ Hz, 3H); LC–MS m/z: 405.2 $[M+H]^+$; $t_R=4.176$ min (Method C); HRMS (ESI+) m/z calcd for $C_{22}H_{25}N_6O_2^+$ 405.2034, found 405.2044; Anal. calcd for $C_{22}H_{24}N_6O_2\cdot1.5\,CF_3COOH$: C 52.18, H 4.47, N 14.60, found C 51.91, H 4.38, N 14.71.

(*R*)-7-Ethyl-5-methyl-2-(2-phenyl-1*H*-imidazol-1-yl)-8-((*R*)-tetrahydrofuran-3-yl)-7,8-dihydropteridin-6(5*H*)-one (15): ^{1}H NMR (400 MHz, $CDCl_3$): $\delta=7.84$ (m, 2H), 7.46–7.62 (m, 6H), 4.19 (dd, $J=7.3$, 2.8 Hz, 1H), 3.92–4.05 (m, 2H), 3.59 (dd, $J=10.0$, 7.8 Hz, 1H), 3.41–3.43 (m, 1H), 3.40 (s, 3H), 3.29 (dd, $J=10.0$, 6.1 Hz, 1H), 1.62–1.92 (m, 4H), 0.82 ppm (t, $J=7.5$ Hz, 3H); LC–MS m/z: 405.2 $[M+H]^+$; $t_R=4.396$ min (Method C); HRMS (ESI+) m/z calcd for $C_{22}H_{25}N_6O_2^+$ 405.2034, found 405.2030.

(*R*)-7-Ethyl-2-(2-(3-fluorophenyl)-1*H*-imidazol-1-yl)-5-methyl-8-((*R*)-tetrahydrofuran-3-yl)-7,8-dihydropteridin-6(5*H*)-one (16): ^{1}H NMR (400 MHz, $CDCl_3$): $\delta=7.89$ (d, $J=2.0$ Hz, 1H), 7.83 (s, 1H), 7.61 (s, 1H), 7.44–7.51 (m, 2H), 7.17–7.25 (m, 2H), 4.01–4.23 (m, 2H), 3.63–3.69 (m, 2H), 3.51 (dd, $J=10.1$, 3.6 Hz, 1H), 3.38–3.34 (m, 1H), 3.35 (s, 3H), 1.65–1.99 (m, 4H), 0.82 ppm (t, $J=7.5$ Hz, 3H); LC–MS m/z: 423.1 $[M+H]^+$; $t_R=4.522$ min (Method C); HRMS (ESI+) m/z calcd for $C_{22}H_{24}FN_6O_2^+$ 423.1939, found 423.1937.

(*R*)-7-Ethyl-2-(2-(4-fluorophenyl)-1*H*-imidazol-1-yl)-5-methyl-8-((*R*)-tetrahydrofuran-3-yl)-7,8-dihydropteridin-6(5*H*)-one (17): ^{1}H NMR (400 MHz, $CDCl_3$): $\delta=7.90$ (s, 1H), 7.81 (s, 1H), 7.57–7.60 (m, 3H), 7.19 (m, 2H), 4.17–4.24 (m, 2H), 3.91–3.99 (m, 1H), 3.66 (dd, $J=10.0$, 7.9 Hz, 1H), 3.55 (dd, $J=9.9$, 2.9 Hz, 1H), 3.44–3.46 (m, 1H), 3.39 (s, 3H), 1.66–2.03 (m, 4H), 0.83 ppm (t, $J=7.5$ Hz, 3H); LC–MS m/z: 423.2 $[M+H]^+$; $t_R=4.837$ min (Method C); HRMS (ESI+) m/z calcd for $C_{22}H_{24}FN_6O_2^+$ 423.1939, found 423.1942.

(*S*)-5,6a-Dimethyl-2-(2-phenyl-1*H*-imidazol-1-yl)-6a,7,8,9-tetrahydropyrrolo[2,1-*h*]pteridin-6(5*H*)-one (18): ^{1}H NMR (400 MHz, $CDCl_3$): $\delta=7.86$ (d, $J=2.7$ Hz, 1H), 7.73 (s, 1H), 7.62 (d, $J=2.7$ Hz, 1H), 7.48 (m, 6H), 3.36 (s, 3H), 3.21 (m, 2H), 2.19 (m, 2H), 2.02 (m, 2H), 1.29 ppm (s, 3H); LC–MS $m/$: 361.1z $[M+H]^+$; $t_R=4.55$ min (Method C); HRMS (ESI+) m/z calcd for $C_{20}H_{21}N_6O^+$ 361.1771, found 361.1768.

(*S*)-6a-Ethyl-5-methyl-2-(2-phenyl-1*H*-imidazol-1-yl)-6a,7,8,9-tetrahydropyrrolo[2,1-*h*]pteridin-6(5*H*)-one (19): The target compound was prepared from **39** and 2-(phenyl)imidazole. The product was purified by HPLC (20–40% CH_3CN/H_2O in 30 min, 20 mL min^{-1}, 210 nm, 0.1% TFA, Phenomenex Luna C_{18}, 2×25 cm); 12 mg of the titled compound was obtained with 99% purity by LC–MS m/z: 375.2 $[M+H]^+$; $t_R=5.24$ (Method C); ^{1}H NMR (400 MHz, $CDCl_3$): $\delta=7.83$ (s, 1H), 7.69 (s, 1H), 7.60–7.42 (m, 6H), 3.25 (s, 3H), 3.21 (m, 1H), 3.14 (m, 1H), 2.00 (m, 2H), 1.90 (m, 2H),

1.76 (m, 1H), 1.57 (m, 1H), 0.77 ppm (t, $J=7.5$ Hz, 3H); HRMS (ESI+) m/z calcd for $C_{21}H_{23}N_6O^+$ 375.1928, found 375.1919.

(*S*)-6a-Ethyl-5-methyl-2-(2-phenyl-1*H*-imidazol-1-yl)-7,8,9,10-tetrahydro-5*H*-pyrido[2,1-*h*]pteridin-6(6a*H*)-one (20): The racemic mixture was resolved by chiral HPLC using an isocratic mixture of EtOH/hexane (1:9, 1 mL min^{-1}) as eluent from a ChiralPak IA column (4.6×250 mm, 5 μm). Under these conditions, compound **20** has a retention time of 13.88 min; ^{1}H NMR (400 MHz, $CDCl_3$): $\delta=7.69$ (s, 1H), 7.65 (s, 1H), 7.47–7.42 (m, 2H), 7.35–7.28 (m, 3H), 7.17 (s, 1H), 3.59 (d, $J=13.4$ Hz, 1H), 3.32 (s, 3H), 2.28 (t, $J=11.6$ Hz, 1H), 2.21 (d, $J=12.6$ Hz, 1H), 2.09 (sext, $J=7.3$ Hz, 1H), 1.86–1.52 (m, 4H), 1.42 (d, $J=13.2$ Hz, 1H), 1.17–1.03 (m, 1H), 0.67 ppm (t, $J=7.4$ Hz, 3H); LC–MS m/z: 389.2 $[M+H]^+$; $t_R=6.85$ (Method C); HRMS (ESI+) m/z calcd for $C_{22}H_{25}N_6O^+$ 389.2084, found 389.2085.

(*S*)-6a-Ethyl-5-methyl-2-(2-phenyl-1*H*-imidazol-1-yl)-6a,7,9,10-tetrahydro[1,4]oxazino[3,4-*h*]pteridin-6(5*H*)-one (21): The purity of **21** was 99% by LC–MS m/z: 390.1 $[M+H]^+$; $t_R=5.24$ min (Method C); ^{1}H NMR (400 MHz, $CDCl_3$): $\delta=7.76$ (s, 1H), 7.73 (s, 1H), 7.44 (m, 1H), 7.33 (m, 4H), 7.18 (s, 1H), 4.13 (d, $J=11.6$ Hz, 1H), 3.72 (d, $J=11.2$ Hz, 1H), 3.61 (d, $J=11.8$ Hz, 1H), 3.35 (s, 3H), 3.23 (m, 2H), 2.63 (m, 1H), 2.23 (m, 1H), 1.91 (m, 1H), 0.74 ppm (t, $J=7.4$ Hz, 3H); HRMS (ESI+) m/z calcd for $C_{21}H_{23}N_6O_2^+$ 391.1877, found 391.1872.

(*R*)-6a-Ethyl-5-methyl-2-(2-phenyl-1*H*-imidazol-1-yl)-6a,7,9,10-tetrahydro[1,4]oxazino[3,4-*h*]pteridin-6(5*H*)-one (*ent*-21): The purity of *ent*-**21** was 99% by LC–MS m/z: 390.1 $[M+H]^+$; $t_R=5.21$ min (Method C); ^{1}H NMR (400 MHz, $CDCl_3$): $\delta=7.75$ (s, 1H), 7.72 (d, $J=2$ Hz, 1H), 7.44 (m, 2H), 7.32 (m, 3H), 7.18 (d, $J=2$ Hz), 4.13 (d, $J=15.5$ Hz, 1H), 3.71 (dd, $J=15.5$, 5.2 Hz, 1H), 3.60 (d, $J=15.5$ Hz, 1H), 3.34 (s, 3H), 3.25–3.14 (m, 2H), 2.62 (m, 1H), 2.25 (m, 1H), 1.92 (m, 1H), 0.72 ppm (t, $J=7.4$ Hz, 3H). The absolute configuration of *ent*-**21** was assigned based on its Plk-2 activity relative to the opposite enantiomer **21**.

(*S*)-6a-Ethyl-5,8-dimethyl-2-(2-phenyl-1*H*-imidazol-1-yl)-7,8,9,10-tetrahydro-5*H*-pyrazino[2,1-*h*]pteridin-6(6a*H*)-one (22): ^{1}H NMR (400 MHz, CD_3OD): $\delta=7.89$ (s, 1H), 7.78 (s, 1H), 7.45–7.30 (m, 5H), 7.13 (s, 1H), 3.50–3.30 (m, 1H), 3.35 (s, 3H), 3.15 (d, $J=11.4$ Hz, 1H), 2.62–2.50 (m, 2H), 2.35–2.25 (m, 1H), 2.25 (s, 3H), 2.13 (d, $J=11.6$ Hz, 1H), 1.90–1.78 (m, 1H), 1.72 (t, $J=11.9$ Hz, 1H), 0.67 ppm (t, $J=7.4$ Hz, 3H); LC–MS m/z: 404.2 $[M+H]^+$; $t_R=13.58$ min (ChiralPak IA 10); (−) rotating enantiomer; HRMS (ESI+) m/z calcd for $C_{22}H_{26}N_7O^+$ 404.2193, found 404.2186.

(*S*)-6a-Ethyl-5-methyl-2-(3-phenylpyridin-4-yl)-6a,7,9,10-tetrahydro[1,4]oxazino[3,4-*h*]pteridin-6(5*H*)-one (23): ^{1}H NMR (400 MHz, $CDCl_3$): $\delta=8.69$ (d, $J=6.8$ Hz, 1H), 8.67 (s, 1H), 7.89 (m, 2H), 7.30 (m, 5H), 7.20 (m, 2H), 4.12 (d, $J=15.4$ Hz, 1H), 3.71 (dd, $J=14.9$, 4.9 Hz, 1H), 3.54 (d, $J=15.4$ Hz, 1H), 3.35 (s, 3H), 3.20 (m, 2H), 2.55 (m, 1H), 2.15 (m, 1H), 1.85 (m, 1H), 0.67 ppm (t, $J=10.1$ Hz, 3H); LC–MS m/z: 402.1 $[M+H]^+$; $t_R=5.886$ min (Method A); HRMS (ESI+) m/z calcd for $C_{23}H_{23}N_5O_2^+$ 402.1925, found 402.1920.

(*S*)-6a-Ethyl-5-methyl-2-(2-phenylpyridin-3-yl)-6a,7,9,10-tetrahydro[1,4]oxazino[3,4-*h*]pteridin-6(5*H*)-one (24): ^{1}H NMR (400 MHz, $CDCl_3$): $\delta=8.74$ (dd, $J=4.8$, 1.7 Hz, 1H), 8.28 (dd, 7.8, 1.7 Hz, 1H), 7.92 (s, 1H), 7.32 (m, 3H), 7.28 (m, 10H), 4.09 (d, $J=11.6$ Hz, 1H), 3.72 (dd, $J=11.5$, 3.7 Hz, 1H), 3.56 (d, $J=11.6$ Hz, 1H), 3.35 (s, 3H), 3.22 (m, 2H), 2.59 (m, 1H), 2.16 (m, 1H), 1.87 (m, 1H), 0.69 ppm (t, $J=7.5$ Hz, 3H); LC–MS m/z: 402.1 $[M+H]^+$; $t_R=5.118$ min (Method A); HRMS (ESI+) m/z calcd for $C_{23}H_{24}N_5O_2^+$ 402.1925, found 402.1921.

(*S*)-6a-Ethyl-5-methyl-2-(5-phenyl-2*H*-1,2,3-triazol-4-yl)-6a,7,9,10-tetrahydro[1,4]oxazino[3,4-*h*]pteridin-6(5*H*)-one (25): To a solution of **42** (0.247 mmol, 0.07 g) in CH_3CN (2 mL) was added $Pd(PPh_3)_4$ (0.007 mmol, 0.008 g), phenylacetylene (0.296 mmol, 0.032 mL), Cu^I (0.007 mmol, 0.001 g), and Et_3N (0.741 mmol, 0.09 mL). The reaction mixture was microwaved for 25 min at 140 °C. The reaction mixture was filtered and concentrated. The resulting residue was purified by flash chromatography (30% EtOAc in hexanes). The resulting residue was dissolved in DMSO (1 mL) and NaN_3 (0.071 mmol, 0.005 g) was added. The reaction mixture was microwaved for 30 min at 175 °C. The reaction mixture was diluted with EtOAc (10 mL), washed with H_2O (10 mL), dried with Na_2SO_4, filtered, and concentrated. The resulting residue was purified by RP-HPLC to provide **25** as a white solid (1.9 mg, 11%); ^{1}H NMR (400 MHz, $CDCl_3$): $\delta=7.96$ (s, 1H), 7.83 (m, 2H), 7.40 (m, 3H), 4.17 (m, 1H), 3.85 (m, 2H), 3.64 (m, 1H), 3.44 (m, 1H), 3.37 (s, 3H), 2.97 (m, 1H), 2.24 (m, 1H), 1.96 (m, 1H), 0.77 ppm (t, $J=7.6$ Hz, 3H); LC–MS m/z: 392.1 $[M+H]^+$; $t_R=2.331$ min (Method A); HRMS (ESI+) m/z calcd for $C_{20}H_{22}N_7O_2^+$ 392.1830, found 392.1823.

(*S*)-6a-Ethyl-5-methyl-2-(3-phenylisoxazol-4-yl)-6a,7,9,10-tetrahydro[1,4]oxazino[3,4-*h*]pteridin-6(5*H*)-one (26): To a solution of intermediate **44** (0.2707 mmol, 0.099 g) in 3 mL DMF wad added *N*,*N*-dimethylformamide dimethylacetal (0.8122 mmol, 0.11 mL). The reaction mixture was stirred at room temperature for 18 h. Hydroxylamine hydrochloride (2.707 mmol, 0.629 g) was added, and the reaction mixture was plunged into a preheated (60 °C) oil bath and was stirred for 1 h. The reaction mixture was cooled to room temperature, diluted with EtOAc, and washed with H_2O. The organic layer was dried over Na_2SO_4, filtered, and concentrated to give a racemic mixture of the compounds. The racemate was resolved by chiral HPLC using an isocratic mixture of EtOH/hexane (3:7, 1 mL min^{-1}) as eluent from a Chiracel OD-H column (0.46×250 mm) to provide compound **26**: ^{1}H NMR (400 MHz, $CDCl_3$): $\delta=8.86$ (s, 1H), 7.98 (m, 2H), 7.89 (s, 1H), 7.44 (m, 3H), 4.22 (d, $J=11.6$ Hz, 1H), 4.00 (dd, $J=13.9$, 2.6 Hz, 1H), 3.91 (dd, $J=11.6$, 3.8 Hz, 1H), 3.66 (d, $J=11.6$ Hz, 1H), 3.51 (m, 1H), 3.35 (s, 3H), 3.04 (m, 2H), 2.26 (m, 1H), 1.99 (m, 1H), 0.79 ppm (t, $J=7.5$ Hz, 3H); LC–MS m/z: 392.1 $[M+H]^+$; $t_R=4.284$ min (Method A); HRMS (ESI+) m/z calcd for $C_{21}H_{22}N_5O_3^+$ 392.1718, found 392.1711.

(*S*)-6a-Ethyl-5-methyl-2-(4-phenyl-1,2,3-thiadiazol-5-yl)-6a,7,9,10-tetrahydro[1,4]oxazino[3,4-*h*]pteridin-6(5*H*)-one (27): To a solution of intermediate **44** (0.2109 mmol, 0.074 g) in 2 mL EtOH, hydrazine (0.707 mmol, 0.023 mL) was added. The reaction mixture was plunged into a preheated (80 °C) oil bath and was stirred for 18 h. The reaction mixture was cooled to room temperature and concentrated. Thionyl chloride (2 mL) was slowly added to the residue. The reaction mixture was stirred for 15 min and then concentrated. The crude mass was dissolved in 10 mL CH_2Cl_2 and washed with saturated aqueous $NaHCO_3$, dried over Na_2SO_4, filtered, and concentrated to give a racemic mixture of the compounds. The racemate was resolved by chiral HPLC using an isocratic mixture of EtOH/hexane (20:80; 1 mL min^{-1}) as eluent with a Chiracel IA 4.6×250 mm column to give isolated **27** and *ent*-**27**. Characterization for **27**: ^{1}H NMR (400 MHz, $CDCl_3$): $\delta=7.83$ (s, 1H), 7.74 (m, 2H), 7.44 (m, 3H), 4.14 (d, $J=11.2$ 1.2 Hz, 1H), 3.84 (m, 1H), 3.62 (m, 2H), 3.40 (m, 1H), 3.35 (s, 3H), 2.84 (m, 1H), 2.23 (m, 1H), 1.97 (m, 1H), 0.76 ppm (t, $J=7.4$ Hz, 3H) LC–MS m/z: 409.0 $[M+H]^+$; $t_R=6.91$ min (Method A); HRMS (ESI+) m/z calcd for $C_{20}H_{21}N_6O_2S^+$ 409.1447, found 409.1433.

(*S*)-2-(2-(2,4-Difluorophenyl)-1*H*-imidazol-1-yl)-6a-ethyl-5-methyl-6a,7,9,10-tetrahydro[1,4]oxazino[3,4-*h*]pteridin-6(5*H*)-one (28): ^{1}H NMR (400 MHz, $CDCl_3$): $\delta = 7.83$ (d, $J = 1.5$ Hz, 1H), 7.72 (s, 1H), 7.67 (m, 1H), 7.22 (d, $J = 1.5$ Hz, 1H), 6.99 (m, 1H), 6.75 (m, 1H), 4.16 (d. $J = 11.7$ Hz, 1H), 3.80 (m, 1H), 3.61 (d, $J = 11.7$ Hz, 1H), 3.34 (m, 5H), 2.76 (m, 1H), 2.26 (m, 1H), 1.94 (m, 1H), 0.75 ppm (t, $J = 7.5$ Hz, 3H); LC–MS *m/z*: 427.1 $[M+H]^+$; $t_R = 2.334$ min (Method A); HRMS (ESI+) *m/z* calcd for $C_{21}H_{21}F_2N_6O_2^+$ 427.1689, found 427.1680.

(*S*)-2-(2-(2,3-Difluorophenyl)-1*H*-imidazol-1-yl)-6a-ethyl-5-methyl-6a,7,9,10-tetrahydro[1,4]oxazino[3,4-*h*]pteridin-6(5*H*)-one (29): ^{1}H NMR (400 MHz, CD_3OD): $\delta = 7.96$ (d, $J = 1.6$ Hz, 1H), 7.91 (s, 1H), 7.44–7.34 (m, 2H), 7.33–7.25 (m, 1H), 7.21 (d, $J = 1.6$ Hz, 1H), 4.02 (d, $J = 11.6$ Hz, 1H), 3.75 (dd, $J = 11.4$, 4.0 Hz, 1H), 3.64 (d, $J = 11.6$ Hz, 1H), 3.37 (dd, $J = 11.8$, 3.2 Hz, 1H), 3.34 (s, 3H), 2.80–2.60 (m, 1H), 2.31 (sext, $J = 7.5$ Hz, 1H), 1.86 (sext, $J = 7.5$ Hz, 1H), 0.72 ppm (t, $J = 7.6$ Hz, 3H); LC–MS *m/z*: 427.1 $[M+H]^+$; $t_R = 6.31$ min (Method C); $t_R = 10.50$ min (ChiralPak IA 10); (+) rotating enantiomer; HRMS (ESI+) *m/z* calcd for $C_{21}H_{21}F_2N_6O_2^+$ 427.1689, found 427.1682.

(*S*)-6a-Ethyl-2-(2-(5-fluoropyridin-2-yl)-1*H*-imidazol-1-yl)-5-methyl-6a,7,9,10-tetrahydro[1,4]oxazino[3,4-*h*]pteridin-6(5*H*)-one (30): ^{1}H NMR (400 MHz, $CDCl_3$): $\delta = 8.54$ (dd, $J = 6.4$, 1.3 Hz, 1H), 8.39 (d, $J = 2.3$ Hz, 1H), 7.87 (d, $J = 1.9$ Hz, 1H), 7.72 (s, 1H), 7.67 (m, 1H), 7.28 (d, $J = 1.9$ Hz, 1H), 4.12 (d, $J = 15.5$ Hz, 1H), 3.78 (dd, $J = 15.3$, 5.3 Hz, 1H), 3.63 (d, 15.6 Hz, 1H), 3.31 (m, 5H), 2.71 (m, 1H), 2.25 (m, 1H), 1.93 (m, 1H), 0.75 ppm (t, $J = 10.0$ Hz, 3H); LC–MS *m/z*: 410.1 $[M+H]^+$; $t_R = 4.775$ min (Method A); HRMS (ESI+) *m/z* calcd for $C_{20}H_{21}FN_7O_2^+$ 410.1735, found 410.1727.

(*S*)-6a-Ethyl-5-methyl-2-(2-(thiazol-2-yl)-1*H*-imidazol-1-yl)-6a,7,9,10-tetrahydro[1,4]oxazino[3,4-*h*]pteridin-6(5*H*)-one (31): ^{1}H NMR (400 MHz, $CDCl_3$): $\delta = 7.80$ (s, 1H), 7.73 (s, 1H), 7.65 (s, 1H), 7.39 (m, 1H), 7.22 (m, 1H), 4.16 (d, $J = 11.6$ Hz, 1H), 3.85 (m, 1H), 3.69 (m, 1H), 3.64 (m, 1H), 3.44 (m, 1H), 3.37 (s, 3H), 2.90 (m, 1H), 2.28 (m, 1H), 1.97 (m, 1H), 0.80 ppm (t, $J = 7.5$ Hz, 3H); LC–MS *m/z*: 398.1 $[M+H]^+$; $t_R = 4.766$ min (Method A); HRMS (ESI+) *m/z* calcd for $C_{18}H_{20}N_7O_2S^+$ 398.1394, found 398.1385.

(*R*)-2-Chloro-8-cyclobutyl-7-ethyl-5-methyl-7,8-dihydropteridin-6(5*H*)-one (33): ^{1}H NMR ($CDCl_3$, 300 MHz): $\delta = 7.67$ (s, 1H), 4.42–4.36 (m, 1H), 4.30–4.27 (m, 1H), 3.32 (s, 3H), 2.58–2.56 (m, 1H), 2.27–2.02 (m, 3H), 1.81–1.58 (m, 4H), 0.84 ppm (t, $J = 4.3$ Hz, 3H); LC–MS *m/z*: 281.0 $[M+H]^+$; $t_R = 9.47$ min (Method B).

(*R*)-2-Chloro-7-ethyl-5-methyl-8-((*R*)-tetrahydrofuran-3-yl)-7,8-dihydropteridin-6(5*H*)-one (35): ^{1}H NMR (400 MHz, $CDCl_3$): $\delta = 7.72$ (s, 1H), 4.79 (m, 1H), 4.23 (dd, $J = 8.0$, 3.8 Hz, 1H), 4.15 (m, 1H), 3.94 (d, $J = 5.6$ Hz, 2H), 3.87 (m, 1H), 3.33 (s, 3H), 2.28 (m, 1H), 2.19 (m, 1H), 1.92 (m, 1H), 1.73 (m, 1H), 0.88 ppm (t, $J = 7.5$ Hz, 3H); LC–MS *m/z*: 345.1 $[M+H]^+$; $t_R = 5.312$ min (Method A).

(*S*)-Methyl 1-(2-chloro-5-nitropyrimidin-4-yl)-2-ethylpyrrolidine-2-carboxylate (38): (*S*)-Methyl 2-ethylpyrrolidine-2-carboxylate (6.16 g, 31.93 mmol) was suspended in THF (100 mL) and the temperature was decreased to 0 °C. *N*,*N*-Diisopropylethylamine (DIPEA; 11.08 mL, 67.05 mmol) was added, and the reaction mixture was stirred for 10 min; 2,4-dichloro-5-nitropyrimidine (6.19 g, 31.93 mmol) was added to the reaction mixture, and the reaction was stirred at 0 °C until complete consumption was observed by TLC. The reaction mixture was diluted with EtOAc and washed with H_2O. The organic layer was dried with anhydrous Na_2SO_4, filtered, and concentrated. The resulting residue was purified by flash chromatography (20% EtOAc in hexanes) to provide title compound (6.16 g, 61%); LC–MS *m/z*: 315.0 $[M+H]^+$; $t_R = 6.093$ min (Method C); ^{1}H NMR (400 MHz, $CDCl_3$): $\delta = 8.73$ (s, 1H), 3.73 (s, 3H), 3.61 (m, 1H), 2.99 (m, 1H), 2.61 (m, 1H), 2.24–2.04 (m, 5H), 0.89 ppm (t, $J = 7.4$ Hz, 3H).

(*S*)-2-Chloro-6a-ethyl-5-methyl-6a,7,8,9-tetrahydropyrrolo[2,1-*h*]pteridin-6(5*H*)-one (39): ^{1}H NMR (300 MHz, $CDCl_3$): $\delta = 7.63$ (s,1H), 3.85 (m, 1H), 3.71 (m, 1H), 3.33 (s, 3H), 2.28 (m, 2H), 2.04 (m, 2H), 1.78 (m,1H), 1.62 (m, 1H), 0.80 ppm (t, $J = 7.5$ Hz, 3H); LC–MS *m/z*: 267.0 $[M+H]^+$; $t_R = 2.781$ min (Method A).

Methyl 4-(2-chloro-5-nitropyrimidin-4-yl)-3-ethylmorpholine-3-carboxylate (41): ^{1}H NMR (400 MHz, $CDCl_3$): $\delta = 8.78$ (s, 1H), 3.87 (m, 4H), 3.75 (s, 3H), 3.54 (m, 1H), 3.04 (m, 1H), 2.48 (m, 1H), 1.97 (m, 1H), 0.86 ppm (t, $J = 7.3$ Hz, 3H); LC–MS *m/z*: 331.0 $[M+H]^+$; $t_R = 4.918$ min (Method A).

2-Chloro-6a-ethyl-5-methyl-6a,7,9,10-tetrahydro[1,4]oxazino[3,4-*h*]pteridin-6(5*H*)-one (42): ^{1}H NMR (400 MHz, $CDCl_3$): $\delta = 7.76$ (s, 1H), 4.34 (dd, $J = 13.9$, 2.8 Hz, 1H), 4.18 (d, $J = 11.7$ Hz, 1H), 4.01 (dd, $J = 11.7$, 3.9 Hz, 1H), 3.66 (d, $J = 11.7$ Hz, 1H), 3.57 (dt, $J = 12.2$, 3.1 Hz, 1H), 3.32 (s, 3H), 3.23 (m, 1H), 2.32 (m, 1H), 2.01 (m, 1H), 0.79 ppm (t, $J = 7.6$ Hz, 3H); LC–MS *m/z*: 282.9 $[M+H]^+$; $t_R = 2.717$ min (Method A).

6a-Ethyl-5-methyl-2-(2-oxo-2-phenylethyl)-6a,7,9,10-tetrahydro-[1,4]oxazino[3,4-*h*]pteridin-6(5*H*)-one (44): Intermediate **42** (0.707 mmol, 0.200 g), sodium methanethiolate (2.12 mmol, 0.148 g) and THF (2 mL) were combined in a sealed tube and heated at 120 °C for 18 h. The reaction mixture was cooled to room temperature, diluted with 15 mL EtOAc, washed with H_2O, dried with Na_2SO_4, filtered and concentrated. The resulting residue was dissolved in 2 mL AcOH, the temperature was decreased to 0 °C, and a solution of $KMnO_4$ (0.848 mmol, 0.134 g) in 2 mL H_2O was added. The reaction mixture was stirred for 2 h at 0 °C, then was quenched with saturated sodium thiosulfate and warmed to room temperature and extracted into EtOAc (3×15 mL). The combined organic layers were dried with Na_2SO_4, filtered, and concentrated. The resulting residue was purified by flash chromatography (50% EtOAc in hexanes) to give 6a-ethyl-5-methyl-2-(methylsulfonyl)-6a,7,9,10-tetrahydro[1,4]oxazino[3,4-*h*]pteridin-6(5*H*)-one.

The above intermediate was added to a suspension of NaH (1.81 mmol, 0.07 g) and acetophenone (1.64 mmol, 0.191 g) in 3 mL THF with stirring at 0 °C. The reaction mixture was stirred for 18 h while slowly warming to room temperature. The reaction mixture was quenched with 10 mL saturated NH_4Cl, diluted with 20 mL of EtOAc, and the two layers were separated. The organic layer was dried with Na_2SO_4, filtered, and concentrated. The resulting residue was purified by flash chromatography (50% EtOAc in hexanes) to provide the title compound as a white solid (0.07 g, 62%): ^{1}H NMR (400 MHz, $CDCl_3$): $\delta = 7.99$ (d, $J = 7.6$ Hz, 1H), 7.81 (m, 2H), 7.40 (m, 3H), 4.39 (s, 1H), 4.19 (m, 1H), 3.95 (m, 1H), 3.61 (m, 1H), 3.50 (m, 1H), 3.32 (s, 3H), 2.19 (m, 1H), 1.93 (m, 1H), 0.79 ppm (t, $J = 7.6$ Hz, 3H); LC–MS *m/z*: 376.2 $[M+H]^+$; $t_R = 2.308$ min (Method A).

Supporting Information

Detailed procedures for the synthesis of compounds **51**, (±)-**22**, (±)-**64**, and (±)-**7**, detailed procedures for the in vitro assays, as well as a full listing of the panel of kinases for inhibition assays by compound **21** are provided in the Supporting Information.

Acknowledgements

We gratefully acknowledge Pam Santiago, Christopher Willits, David Chian, and Erich Goldbach for their skillful support. We especially thank John Erve for the determination of HRMS data for all final compounds.

Keywords: computational chemistry · kinase inhibitors · medicinal chemistry · Parkinson's disease · polo-like kinase-2

[1] E. Kövari, J. Horvath, C. Bouras, *Brain Res. Bull.* **2009**, *80*, 203 – 210.
[2] a) H. Fujiwara, M. Hasegawa, N. Dohmae, A. Kawashima, E. Masliah, M. S. Goldberg, J. Shen, K. Takio, T. Iwatsubo, *Nat. Cell Biol.* **2002**, *4*, 160 – 164; b) Y. Saito, A. Kawashima, N. N. Ruberu, H. Fujiwara, S. Koyama, M. Sawabe, T. Arai, H. Nagura, H. Yamanouchi, M. Hasegawa, T. Iwatsubo, S. Murayama, *J. Neuropathol. Exp. Neurol.* **2003**, *62*, 644 – 654; c) J. P. Anderson, D. E. Walker, J. M. Goldstein, R. de Laat, K. Banducci, R. J. Caccavello, R. Barbour, J. Huang, K. Kling, M. Lee, L. Diep, P. S. Keim, X. Shen, T. Chataway, M. G. Schlossmacher, P. Seubert, D. Schenk, S. Sinha, W. P. Gai, T. J. Chilcote, *J. Biol. Chem.* **2006**, *281*, 29739 – 29752.
[3] K. J. Inglis, D. Chereau, E. F. Brigham, S. S. Chiou, S. Schobel, N. L. Frigon, M. Yu, R. J. Caccavello, S. Nelson, R. Motter, S. Wright, D. Chian, P. Santiago, F. Soriano, C. Ramos, K. Powell, J. M. Goldstein, M. Babcock, T. Yednock, F. Bard, G. S. Basi, H. Sham, T. J. Chilcote, L. McConlogue, I. Griswold-Prenner, J. P. Anderson, *J. Biol. Chem.* **2009**, *284*, 2598 – 2602.
[4] M. K. Mbefo, K. E. Paleologou, A. Boucharaba, A. Oueslati, H. Schell, M. Fournier, D. Olschewski, G. Yin, M. Zweckstetter, E. Masliah, P. J. Kahle, H. Hirling, H. A. Lashuel, *J. Biol. Chem.* **2010**, *285*, 2807 – 2822.
[5] a) M. Takahashi, H. Kanuka, H. Fujiwara, A. Koyama, M. Hasegawa, M. Miura, T. Iwatsubo, *Neurosci. Lett.* **2003**, *336*, 155 – 158; b) M. Neumann, P. J. Kahle, B. I. Giasson, L. Ozmen, E. Borroni, W. Spooren, V. Muller, S. Odoy, H. Fujiwara, M. Hasegawa, T. Iwatsubo, J. Q. Trojanowski, H. A. Kretzschmar, C. Haass, *J. Clin. Invest.* **2002**, *110*, 1429 – 1439; c) P. J. Kahle, M. Neumann, L. Ozmen, V. Muller, H. Jacobsen, W. Spooren, B. Fuss, B. Mallon, W. B. Macklin, H. Fujiwara, M. Hasegawa, T. Iwatsubo, H. A. Kretzschmar, C. Haass, *EMBO Rep.* **2002**, *3*, 583 – 588.
[6] B. C. van de Weerdt, R. H. Medema, *Cell Cycle* **2006**, *5*, 853 – 864.
[7] a) V. Archambault, D. M. Glover, *Nat. Rev. Mol. Cell Biol.* **2009**, *10*, 265 – 275; b) K. Strebhardt, *Nat. Rev. Drug Discovery* **2010**, *9*, 643 – 660.
[8] a) E. F. Johnson, K. D. Stewart, K. W. Woods, V. L. Giranda, Y. Luo, *Biochemistry* **2007**, *46*, 9551 – 9563; b) M. Steegmaier, M. Hoffmann, A. Baum, P. Lenart, M. Petronczki, M. Krssak, U. Gurtler, P. Garin-Chesa, S. Lieb, J. Quant, M. Grauert, G. R. Adolf, N. Kraut, J. M. Peters, W. J. Rettig, *Curr. Biol.* **2007**, *17*, 316 – 322; c) K. Strebhardt, A. Ullrich, *Nat. Rev. Cancer* **2006**, *6*, 321 – 330.
[9] a) M. Kothe, D. Kohls, S. Low, R. Coli, A. C. Cheng, S. L. Jacques, T. L. Johnson, C. Lewis, C. Loh, J. Nonomiya, A. L. Sheils, K. A. Verdries, T. A. Wynn, C. Kuhn, Y. H. Ding, *Biochemistry* **2007**, *46*, 5960 – 5971; b) T. M. Bandeiras, R. C. Hillig, P. M. Matias, U. Eberspaecher, J. Fanghanel, M. Thomaz, S. Miranda, K. Crusius, V. Putter, P. Amstutz, M. Gulotti-Georgieva, H. K. Binz, C. Holz, A. A. Schmitz, C. Lang, P. Donner, U. Egner, M. A. Carrondo, B. Muller-Tiemann, *Acta Crystallogr. Sect. D* **2008**, *64*, 339 – 353.
[10] Z. Andrysik, W. Z. Bernstein, L. Deng, D. L. Myer, Y. Q. Li, J. A. Tischfield, P. J. Stambrook, El M. Bahassi, *Nucleic Acids Res.* **2010**, *38*, 2931 – 2943.
[11] a) S. Ma, J. Charron, R. L. Erikson, *Mol. Cell Biol.* **2003**, *23*, 6936 – 6943; b) Y. Yang, J. Bai, R. Shen, S. A. Brown, E. Komissarova, Y. Huang, N. Jiang, G. F. Alberts, M. Costa, L. Lu, J. A. Winkles, W. Dai, *Cancer Res.* **2008**, *68*, 4077 – 4085.
[12] a) S. Warnke, S. Kemmler, R. S. Hames, H. L. Tsai, U. Hoffmann-Rohrer, A. M. Fry, I. Hoffmann, *Curr. Biol.* **2004**, *14*, 1200 – 1207; b) T. F. Burns, P. Fei, K. A. Scata, D. T. Dicker, W. S. El-Deiry, *Mol. Cell Biol.* **2003**, *23*, 5556 – 5571.
[13] a) T. Matsumoto, P.-y. Wang, W. Ma, H. J. Sung, S. Matoba, P. M. Hwang, *Proc. Natl. Acad. Sci. USA* **2009**, *106*, 14542 – 14546; b) M. Raab, S. Kappel, A. Kramer, M. Sanhaji, Y. Matthess, E. Kurunci-Csacsko, J. Calzada-Wack, B. Rathkolb, J. Rozman, T. Adler, D. H. Busch, I. Esposito, H. Fuchs, V. Gailus-Durner, M. Klingenspor, E. Wolf, N. Sanger, F. Prinz, M. H. Angelis, J. Seibler, J. Yuan, M. Bergmann, R. Knecht, B. Kreft, K. Strebhardt, *Nat. Commun.* **2011**, *2*, 395.
[14] a) D. P. Seeburg, M. Feliu-Mojer, J. Gaiottino, D. T. Pak, M. Sheng, *Neuron* **2008**, *58*, 571 – 583; b) G. Kauselmann, M. Weiler, P. Wulff, S. Jessberger, U. Konietzko, J. Scafidi, U. Staubli, J. Bereiter-Hahn, K. Strebhardt, D. Kuhl, *EMBO J.* **1999**, *18*, 5528 – 5539.
[15] L. X. Wu, C. K. Sun, Y. M. Zhang, M. Fan, J. Xu, H. Ma, J. Zhang, *Brain Res.* **2007**, *1168*, 38 – 45.
[16] D. M. Evers, J. A. Matta, H. S. Hoe, D. Zarkowsky, S. H. Lee, J. T. Isaac, D. T. Pak, *Nat. Neurosci.* **2010**, *13*, 1199 – 1207.
[17] W. C. Zimmerman, R. L. Erikson, *Cell Cycle* **2007**, *6*, 1314 – 1318.
[18] D. T. Pak, M. Sheng, *Science* **2003**, *302*, 1368 – 1373.
[19] S. Bowers, A. P. Truong, M. Ye, D. L. Aubele, J. M. Sealy, R. J. Neitz, R. K. Hom, W. Chan, M. S. Dappen, R. A. Galemmo, Jr., A. W. Konradi, H. L. Sham, Y. L. Zhu, P. Beroza, G. Tonn, H. Zhang, J. Hoffman, R. Motter, D. Fauss, P. Tanaka, M. P. Bova, Z. Ren, D. Tam, L. Ruslim, J. Baker, D. Pandya, L. Diep, K. Fitzgerald, D. R. Artis, J. P. Anderson, M. Bergeron, *Bioorg. Med. Chem. Lett.* **2013**, *23*, 2743 – 2749.
[20] a) "Pyridodihydropyraziones, process for their manufacture and use thereof as medicaments": T. Brandl, M. Grauert, R. Hauptmann, M. Hoffmann, M. Steegmaier, (Boehringer Ingelheim International GmbH), US7625899 B2, **2009**; b) "Dihydropteridinones, method for the production and use thereof in the form of drugs": A. Baum, T. Brandl, S. Breitfelder, F. Colbatzky, C. Eickmeier, M. Grauert, M. Hoffmann, J. J. Quant, G. Schnapp, F. Solca, M. Steegmaier, (Boehringer Ingelheim Pharma GmbH & Co. Kg), Int. Pat. Appl. WO2004076454 A1, **2004**; c) "Method for the Production of Dihydropteridinones": G. Linz, G. F. Kraemer, L. Gutschera, G. Asche, (Boehringer Ingelheim International GmbH), Int. Pat. Appl. WO 2006018220A2, **2006**; d) G. Budin, K. S. Yang, T. Reiner, R. Weissleder, *Angew. Chem.* **2011**, *123*, 9550 – 9553; *Angew. Chem. Int. Ed.* **2011**, *50*, 9378 – 9381.
[21] M. Kothe, D. Kohls, S. Low, R. Coli, G. R. Rennie, F. Feru, C. Kuhn, Y. H. Ding, *Chem. Biol. Drug Des.* **2007**, *70*, 540 – 546.
[22] C. Bissantz, B. Kuhn, M. Stahl, *J. Med. Chem.* **2010**, *53*, 5061 – 5084.
[23] W. B. Jennings, B. M. Farrell, J. F. Malone, *Acc. Chem. Res.* **2001**, *34*, 885 – 894.
[24] A. P. Truong, D. L. Aubele, G. D. Probst, M. L. Neitzel, C. M. Semko, S. Bowers, D. Dressen, R. K. Hom, A. W. Konradi, H. L. Sham, A. W. Garofalo, P. S. Keim, J. Wu, M. S. Dappen, K. Wong, E. Goldbach, K. P. Quinn, J. M. Sauer, E. F. Brigham, W. Wallace, L. Nguyen, S. S. Hemphill, M. P. Bova, F. Bard, T. A. Yednock, G. Basi, *Bioorg. Med. Chem. Lett.* **2009**, *19*, 4920 – 4923.
[25] a) J. Srinivasan, T. E. Cheatham, P. Cieplak, P. A. Kollman, D. A. Case, *J. Am. Chem. Soc.* **1998**, *120*, 9401 – 9409; b) Y. N. Vorobjev, J. C. Almagro, J. Hermans, *Proteins* **1998**, *32*, 399 – 413; c) B. Jayaram, D. Sprous, M. A. Young, D. L. Beveridge, *J. Am. Chem. Soc.* **1998**, *120*, 10629 – 10633; d) P. A. Kollman, I. Massova, C. Reyes, B. Kuhn, S. Huo, L. Chong, M. Lee, T. Lee, Y. Duan, W. Wang, O. Donini, P. Cieplak, J. Srinivasan, D. A. Case, T. E. Cheatham III, *Acc. Chem. Res.* **2000**, *33*, 889 – 897.
[26] While the absolute configuration of the ethyl group at position 7 of the pteridinone ring has been firmly established by the X-ray co-crystal structures and precedence of BI 2536, the absolute stereochemical configurations shown for the tetrahydrofuran ring appended to the 8-position of **13**, and **14**–**16** had to be assigned arbitrarily. All attempts to determine the absolute stereochemical configuration of the tetrahydrofuran ring in **14**, and **15**–**17** or one of the synthetic intermediates by single-crystal X-ray crystallography were unsuccessful.
[27] a) S. V. Ley, A. W. Thomas, *Angew. Chem.* **2003**, *115*, 5558 – 5607; *Angew. Chem. Int. Ed.* **2003**, *42*, 5400 – 5449; b) P. Wang, C. Liang, M. Leung, *Tetrahedron* **2005**, *61*, 2931 – 2939.
[28] G. D. I. Artman, R. J. Rafferty, R. M. Williams, *Org. Synth.* **2009**, *86*, 262 – 273.
[29] J. J. Jagodzinski, D. L. Aubele, D. A. Quincy, M. S. Dappen, R. K. Hom, R. A. Galemmo, Jr., A. W. Konradi, H. L. Sham, *Tetrahedron Lett.* **2011**, *52*, 2471 – 2472.
[30] R. Vancraenenbroeck, E. Lobbestael, M. D. Maeyer, V. Baekelandt, J. M. Taymans, *CNS Neurol. Disord. Drug Targets* **2011**, *10*, 724 – 740.
[31] M. K. Lee in *Parkinson's Disease: Genetics and Pathogenesis* (Ed.: T. M. Dawson), Informa Healthcare USA Inc., **2007**, pp. 251 – 268.
[32] a) D. Kirik, A. Bjorklund, *Trends Neurosci.* **2003**, *26*, 386 – 392; b) M. F. Chesselet, *Exp. Neurol.* **2008**, *209*, 22 – 27.

[33] "Processing of X-ray Diffraction Data Collected in Oscillation Mode": Z. Otwinowski, W. Minor in *Methods in Enzymology, Vol. 276* (Eds.: C. W. Carter, Jr., R. M. Sweet), Academic Press, New York, **1997**, pp. 307 – 326.
[34] "Coot News": B. Lohkamp, P. Emsley, K. Cowtan in *CCP4 Newsletter on Protein Crystallography, No. 42*, **2005**: http://www.ccp4.ac.uk/newsletters/newsletter42.pdf (accessed May 26, 2013).
[35] G. N. Murshudov, A. A. Vagin, E. J. Dodson, *Acta Crystallogr. Sect. D* **1997**, *53*, 240 – 255.
[36] D. A. Case, T. A. Darden, T. E. Cheatham III, C. L. Simmerling, J. Wang, R. E. Duke, R. Luo, M. Crowley, R. C. Walker, W. Zhang, K. M. Merz, B. Wang, S. Hayik, A. Roitberg, G. Seabra, I. Kolossváry, K. F. Wong, F. Paesani, J. Vanicek, X. Wu, S. R. Brozell, T. Steinbrecher, H. Gohlke, L. Yang, C. Tan, J. Mongan, V. Hornak, G. Cui, D. H. Mathews, M. G. Seetin, C. Sagui, V. Babin, P. A. Kollman, AMBER 10, University of California, San Francisco, **2008**.
[37] J. Wang, W. Wang, P. A. Kollman, D. A. Case, *J. Mol. Graphics Modell.* **2006**, *25*, 247 – 260.
[38] a) M. E. Voss, C. M. Beer, S. A. Mitchell, P. A. Blomgren, P. E. Zhichkin, *Tetrahedron* **2008**, *64*, 645 – 651; b) R. P. Frutos, I. Gallou, D. Reeves, Y. Xu, D. Krishnamurthy, C. H. Senanayake, *Tetrahedron Lett.* **2005**, *46*, 8369 – 8372.

Received: April 16, 2013
Published online on ■■ ■■, 0000